NASA Contractor Report 172283

Development of an Advanced Pitch Active Control System and a Reduced Area Horizontal Tail for a Wide Body Jet Aircraft

Executive Summary

Wiley A. Guinn

LOCKHEED-CALIFORNIA COMPANY
BURBANK, CALIFORNIA

CONTRACT NO. NAS1-15326

National Aeronautics and
Space Administration

Langley Research Center
Hampton, Virginia 23665

NASA Contractor Report 172283

Development of an Advanced Pitch Active Control System and a Reduced Area Horizontal Tail for a Wide Body Jet Aircraft

Executive Summary

Wiley A. Guinn

LOCKHEED-CALIFORNIA COMPANY
BURBANK, CALIFORNIA

CONTRACT NO. NAS1-153[illegible]

National Aeronautics and
Space Administration

Langley Research Center
Hampton, Virginia 23665

SUMMARY

Commercial transport aircraft fuel consumption can be significantly reduced by relaxing the longitudinal static stability and by decreasing the size of the horizontal tail. However, both of these fuel saving concepts usually result in degraded aircraft flying qualities. The flying qualities can be restored by using a Pitch Active Control System (PACS) to provide stability augmentation.

This report summarizes work that was accomplished for the NASA Aircraft Energy Efficiency program by Lockheed toward development of an advanced pitch active control system (NASA CR 172277) and a reduced area horizontal tail (NASA CR 172278) for a commercial widebody transport (L-1011).

The advanced PACS design objective was to develop a longitudinal pitch active control system for an advanced transport configuration that would provide satisfactory flying qualities to a negative 10% static stability margin. The major program tasks were development of the control laws, validation of the control laws by piloted flight simulation tests, and development of the advanced PACS architecture that would be suitable for a flight test demonstration program. All of these tasks were successfully accomplished. The modal control method of modern control theory was used for control law development. The control laws were initially verified by flying qualities analysis. Then, piloted flight simulation tests, which were performed on the NASA Langley visual motion simulator, demonstrated the validity of the control laws. As the center of gravity (c.g.) location was moved aft of 35 percent on the baseline aircraft (PACS off), the pilot ratings degraded rapidly to the threshold of unacceptability at the neutral point. Engagement of the PACS for c.g. locations at the natural point and aft to negative stability margins of 20 percent mac provided flying qualities equivalent to those of the baseline aircraft at a positive 15 percent stability margin. The PACS architecture required either dual, triple or quadruple sensor inputs to a quadruple channel digital computer which provided command signals to two single channel series servos with limited control authority.

The reduced area horizontal tail design objective was to determine the maximum drag benefit that can be achieved by reducing the L-1011 tail area. The program included evaluation of four small horizontal tail concepts with planform areas on 30 and 38 percent less than the standard L-1011 tail. Profile changes which were evaluated included leading edge radius, camber, thickness to chord ratio, and high-lift devices. Planform changes evaluated were tip configuration, leading edge sweep, aspect ratio, and taper ratio. Included in the report are results of the high-speed and low-speed wind tunnel tests. An airplane drag reduction of approximately two percent was obtained with the best small tail design. However, forward c.g. limitations would have to be imposed on the aircraft because the maximum horizontal tail lift goal was not achieved and sufficient aircraft nose-up control authority was not available. This limitation would not be required for a properly designed new aircraft.

TABLE OF CONTENTS

TABLE OF CONTENTS (Continued)

LIST OF FIGURES

LIST OF FIGURES (Continued)

LIST OF TABLES

LIST OF SYMBOLS

A	State-space equation dynamic matrix of aerodynamic data
AACS	Aileron active control system
A/C	Aircraft
ACEE	Aircraft Energy Efficiency
AFCS	Automatic flight control system
B	State-space equation input distribution matrix
C	State-space equation output distribution matrix
C*	Blended normal-acceleration/pitch-rate parameter
C_D	Aircraft drag coefficient
C_F	L-1011 longitudinal control system feel spring
C_L	Airfoil lift coefficient
$C_{L_{DES}}$	Design airfoil lift coefficient
C_{L_H}	Horizontal tail lift coefficient
$C_{L_{max}}$	Maximum tail lift coefficient
C_m	Pitching moment coefficient
C_ϕ	Coefficient of the bank angle term for secondary gain scheduling
c.g.	Aircraft center of gravity
c.p.	Wing center of pressure
D	State-space equation feed-forward matrix, or drag
deg	Degrees
F	State-space equation feedback matrix

F_C	Control column force
FCES	Flight control electronic system panel
ft	Feet
g	Acceleration of gravity
G_1	Computed feedback gains
G_2	J-curve compensated feedback gains
G_3	Computed feed-forward gains
G_4	Computed feedback gains after elimination of velocity sensor signal
G_5	Scheduled gains (feed-forward and feedback)
h	Altitude
in.	Inches
J	J-curve (relationship between control column displacement and horizontal stabilizer rotation)
J'	Space derivative of J-curve
K_c	Normalizing constant = 2.5
K_{FF}	Feed-forward gain
K_M	Mach gain
K_{N_Z}	Normal acceleration gain
K_u	Velocity gain
K_α	Angle of attack augmented gain
K_θ	Pitch attitude gain
$K_{\dot{\theta}}$	Pitch rate gain
K_ϕ	Bank angle augmented gain
K_3	Combined pitch-attitude/velocity gain
KEAS	Knots equivalent air speed

Kt	Knots
L	Aircraft Aerodynamic lift force
lbs	Pounds
LSWT	Low speed wing tunnel
L-1011	Lockheed wide body commercial transport
M	Mach number
mac	Mean aerodynamic chord
MCT	Maximum continuous thrust
MTO	Maximum takeoff thrust
N_Z	Normal acceleration feedback signal
N_{Z_F}	Filtered normal acceleration feedback signal
N.C.	Numerical controlled
PACS	Pitch active control system
PLF	Power for level flight
PT	Pressure wind tunnel
q	Dynamic pressure
rad	Radian
RSS	Relaxed static stability
s	Laplace transform parameter
S.L.	Sea level
sec	Second
S/N	Serial number
SW	switch
TPT	Transonic pressure wind tunnel
T/ST	Transonic/supersonic wind tunnel

u	State-space equation input vector
V	Aircraft equivalent air speed
V_{mo}	Aircraft maximum operating speed
V_s	Aircraft stall speed
W	Aircraft weight
w	Input vector from pilot
x	State vector
$\dot{x}$	Time derivative of state vector
X_A	Electronic input signal to series servo
X_C	Control column displacement
X_S	Output displacement of series servo
X_T	Output displacement of column trim
x_o	Initial dynamic state of aircraft
y	State-space equation feedback signals
α	Angle of attack
α_{FRL}	Angle of attack relative to fuselage reference line
δ	Pressure of air at aircraft altitude/pressure of air at sea level
S_{A_C}	Outboard aileron symmetrical deflection
δ_e	Elevator deflection
δ_F	Wing flap deflection
δ_H	Horizontal stabilizer angle
$\dot{\delta}_H$	Horizontal stabilizer angular velocity
δ_{H_C}	Horizontal stabilizer command signal
δ_{HT}	Horizontal stabilizer trim angle

δ^*_{HT}	Modified horizontal stabilizer feedback gain signal for secondary gain scheduling
ΔC_{D_H}	Horizontal tail drag increment
$\Delta\delta_c$	Mach trim compensation
$\Delta\delta_o$	Mach trim servo offset schedule
ζ	Short-period and phugoid mode damping
ζ_{SP}	Short-period mode damping
η_L	Dynamic pressure at horizontal tail
η	Aircraft load factor
θ	Pitch attitude feedback signal
$\dot{\theta}$	Pitch rate feedback signal
$\dot{\theta}_F$	Filtered pitch rate feedback signal
λ_i	State-space equation eigenvalues
ν_i	State-space equation eigenvectors
τ_c	Force sensor filter time constant
τ_M	Mach trim compensation filter time constant
τ_P	Power actuator time constant
τ_S	Series servo time constant
τ_Z	Normal acceleration feedback signal filter time constant
$\tau_{\dot{\theta}}$	Pitch rate feedback signal filter time constant
τ_1	Numerator time constant of lag-lead transfer function
τ_2	Denominator time constant of lag-lead transfer function
ϕ	Bank angle or phase angle on Nyquist diagrams
ω	Short-period or phugoid mode circular frequency
ω_{SP}	Short-period mode circular frequency
ω_o	Reference short-period mode circular frequency for the specific flight condition

1. INTRODUCTION

1.1 Background

Jet aircraft fuel cost has increased from about 12 cents per gallon in 1972 to about $1.00 a gallon in 1983. As a result, the fuel cost portion of aircraft direct operating cost has increased from 25 percent to nearly 60 percent. This trend was recognized early by aircraft manufacturers and government leaders. Therefore, in 1975 the U.S. Congress requested NASA to implement a program to develop fuel saving technology for commercial transports.

The NASA Aircraft Energy Efficiency (ACEE) program was initiated in 1976. Since the Lockheed California Company was manufacturing a wide body commercial transport (L-1011) and had been developing active control technology since 1972, Lockheed received an ACEE program contract in February 1977 for "Development and Flight Evaluation of Active Control Concepts for Subsonic Transport Aircraft" (NASA Contract NAS1-14690). The contract resulted in the development of an aileron active control system (AACS) which provided wing load alleviation. The AACS allowed a 5.8 percent wing span increase for the L-1011-500 (in service date 1980) which decreased fuel consumption by approximately three percent (Reference 1). Also, studies were conducted under the contract to evaluate benefits of a pitch active control system (PACS). Piloted flight simulation tests were conducted on a moving base simulator with an L-1011 cab. These tests showed that a lagged pitch rate damper provided flying qualities with static longitudinal stability relaxed to near neutral and in heavy turbulence that are equivalent to those of the baseline aircraft. The aft c.g. simulation results provided a sufficient basis for proceeding to a flight evaluation of the defined augmentation control laws with relaxed static stability.

In December 1978 Lockheed was awarded a second ACEE program contract (NAS1-15326) for "Development and Flight Evaluation of an Augmented Stability Active Controls Concept with a Small Horizontal Tail". In May 1980 the program was restructured to develop a PACS for improvement of flying qualities at aft c.g. flight conditions utilizing a standard L-1011 tail and to continue small tail drag reduction evaluation by analyses and wind-tunnel tests. The PACS development program was divided into two parts: a near-term PACS with capability to provide satisfactory flying qualities to near neutral stability within the linear stability flight region, and an advanced PACS with capability to provide satisfactory flying qualities for negative static stability margins of 10 percent mean aerodynamic chord (mac) throughout the aircraft flight envelope. The near-term PACS part of the program was successfully completed and is reported in Reference 2 and Reference 3 Extended Work CR-172266. The advanced PACS part of the program is documented in Reference 4 and the small tail program results is documented in Reference 5.

1.2 Program Objectives

The program overall objective was to develop fuel saving technology for commercial transport aircraft. The goals were to achieve a four percent fuel saving by c.g. management for aircraft with advanced wing configurations (Figure 1) and to achieve a three percent fuel savings by reducing the horizontal tail size (Figure 2).

The advanced PACS program objective was to develop a high reliability pitch active control system for a future commercial transport that provides handling qualities at a negative 10% static stability margin which are equivalent to those of the baseline L-1011 with the c.g. at 25 percent mac (+15% static margin). The L-1011 has good handling qualities at this c.g. location.

The small tail program objective was to determine the maximum drag benefit that can be achieved by reducing the horizontal tail area. The reduced area must be consistent with moving the c.g. range aft and the controllability requirements.

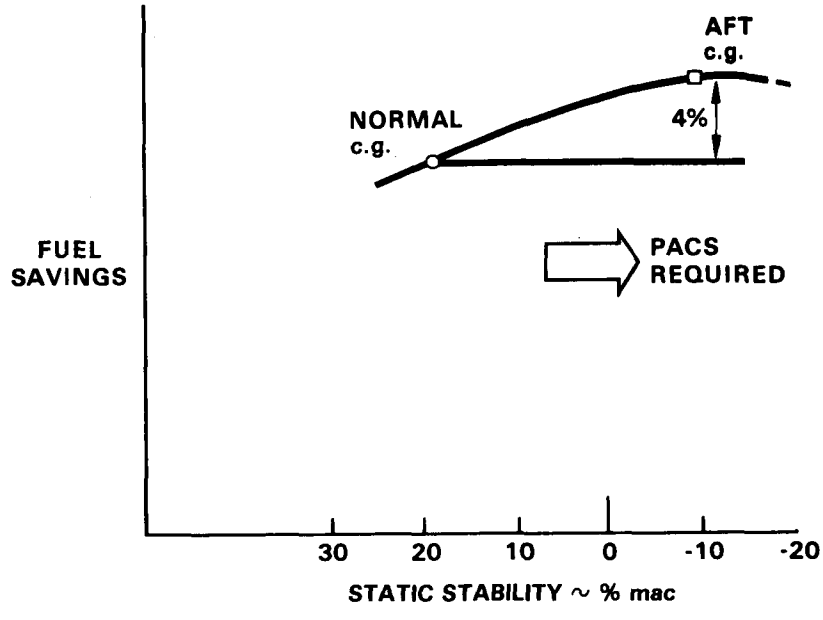

Figure 1. - c.g. management system fuel savings.

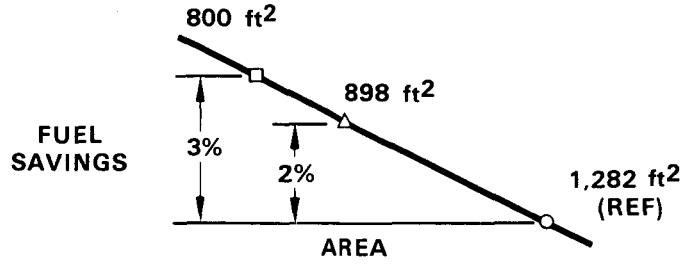

Figure 2. - Reduced area horizontal tail fuel savings.

1.3 Scope of Program

The advanced PACS program consisted of design criteria definition, control law synthesis, flying quality analysis, piloted flight simulation tests, and system architecture specification.

The small tail program consisted of design criteria definition, design and fabrication of the reduced area horizontal tail models, and wind tunnel tests.

2. ADVANCED PACS DEVELOPMENT

The Lockheed L-1011 house airplane (S/N 1001) was used as the basis for design of the advanced PACS. This airplane (Figure 3) is an L-1011-1 model except for the extended wing tips and active control ailerons which are installed on the L-1011-500 models. The airplane has a flying stabilizer with a geared elevator which has been downrigged five degrees to provide the required nose down authority when the c.g. is moved aft to allow flight at negative static stability margins to three percent mac. Center of gravity (c.g.) management is provided by an electrically controlled water ballast system for performance of flight tests (Reference 2).

A block diagram which shows the major elements of the L-1011 longitudinal control system with the advanced PACS installed is given in Figure 4. The dashed lines represent the baseline aircraft longitudinal controls and the solid lines represent the advanced PACS. Input signals to the controller are defined in Table 1. The system has dual series servos for safety reasons. Failure of one servo will not induce a swift elevator deflection (hardover) which will over stress the aircraft. A schematic of the L-1011 control system with the series servos (black lines) installed is shown in Figure 5.

2.1 Control Law Design Objectives

Design objectives for control law synthesis included dynamic stability, maneuver stability, and normal-acceleration/pitch-rate response as shown in Figures 6, 7, and 8 respectively. Speed stability was not included in the initial design objectives. However, speed stability analysis (Section 2.3.3) established a requirement for using this design objective in future control law development programs.

2.2 Control Law Synthesis

The entire discussion in this section is based on the block diagram for control law synthesis given in Figure 9.

The synthesis process started with a separate set of aerodynamic data (trim conditions and stability derivatives) for each of the flight cases listed in Table 2. The aerodynamic data was input to the baseline aircraft model.

2.2.1 Feedback Loop Gain.- Development of the feedback loop gains consisted of the following steps.

- Determining a reference eigenstructure (λ_i, ν_i) for each flight condition from the baseline aircraft model
- Computing the feedback gains matrix (G_1) by utilizing modal control synthesis

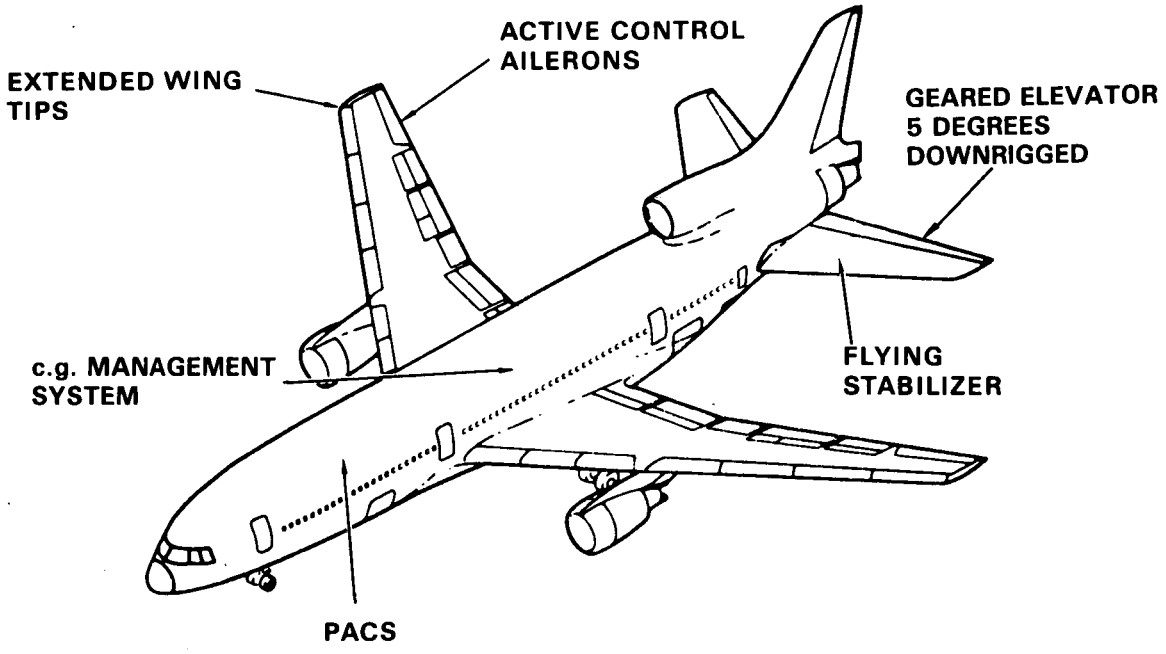

Figure 3. - Flight test airplane (L-1011 S/N 1001).

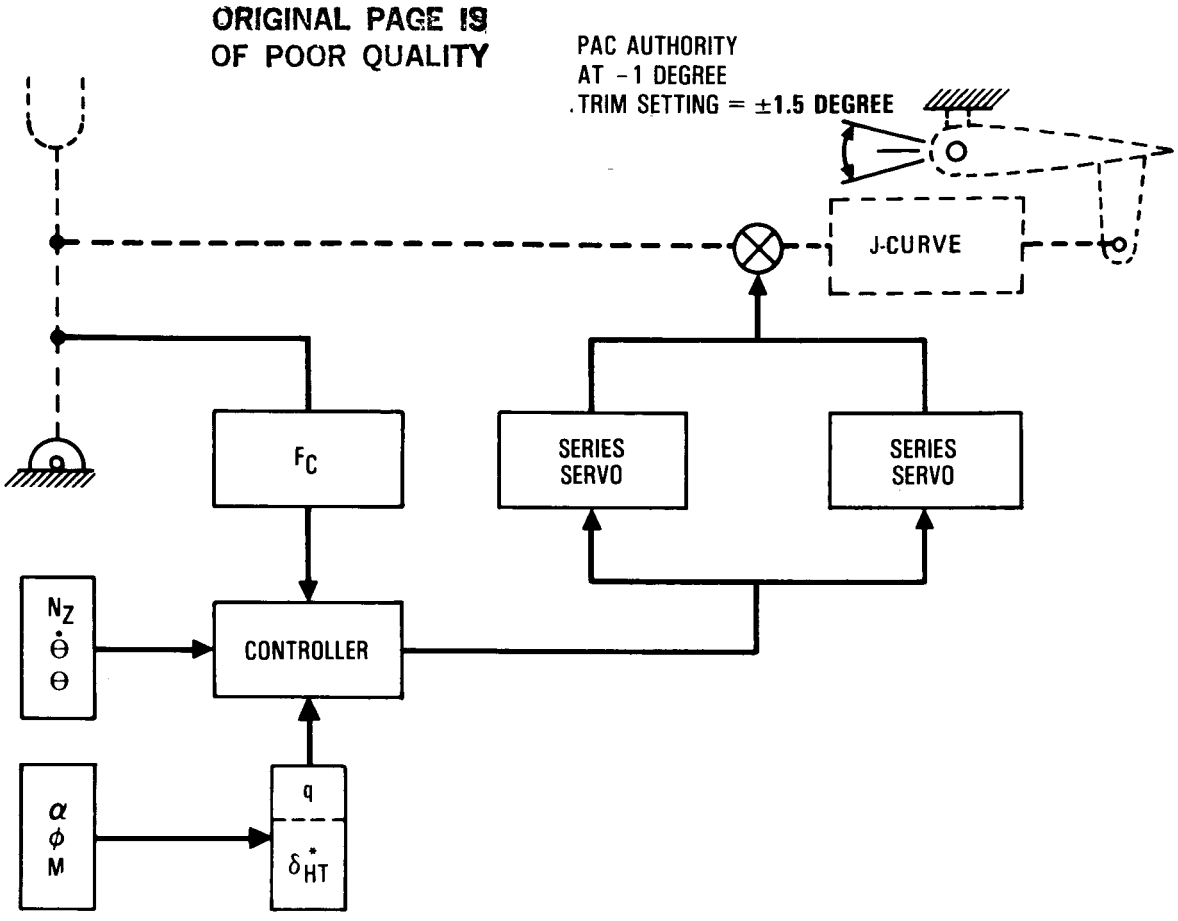

Figure 4. - Longitudinal control system with the advanced PACS.

TABLE 1. - PACS CONTROLLER INPUT SIGNALS

SYMBOL	SIGNAL	TYPE	USE
F_C	Column force	Feed-forward	Column force gradient
N_Z	Normal acceleration	Feedback	Short period mode
$\dot{\theta}$	Pitch rate		
θ	Pitch attitude		Phugoid mode
q	Dynamic pressure	Primary gain scheduling	Compensation for flight condition changes
δ^*_{HT}	Horizontal stabilizer trim		
α	Angle of attack	Secondary gain scheduling	Compensation for pitch-up and AACS outboard aileron operation
ϕ	Bank angle		
M	Mach number		

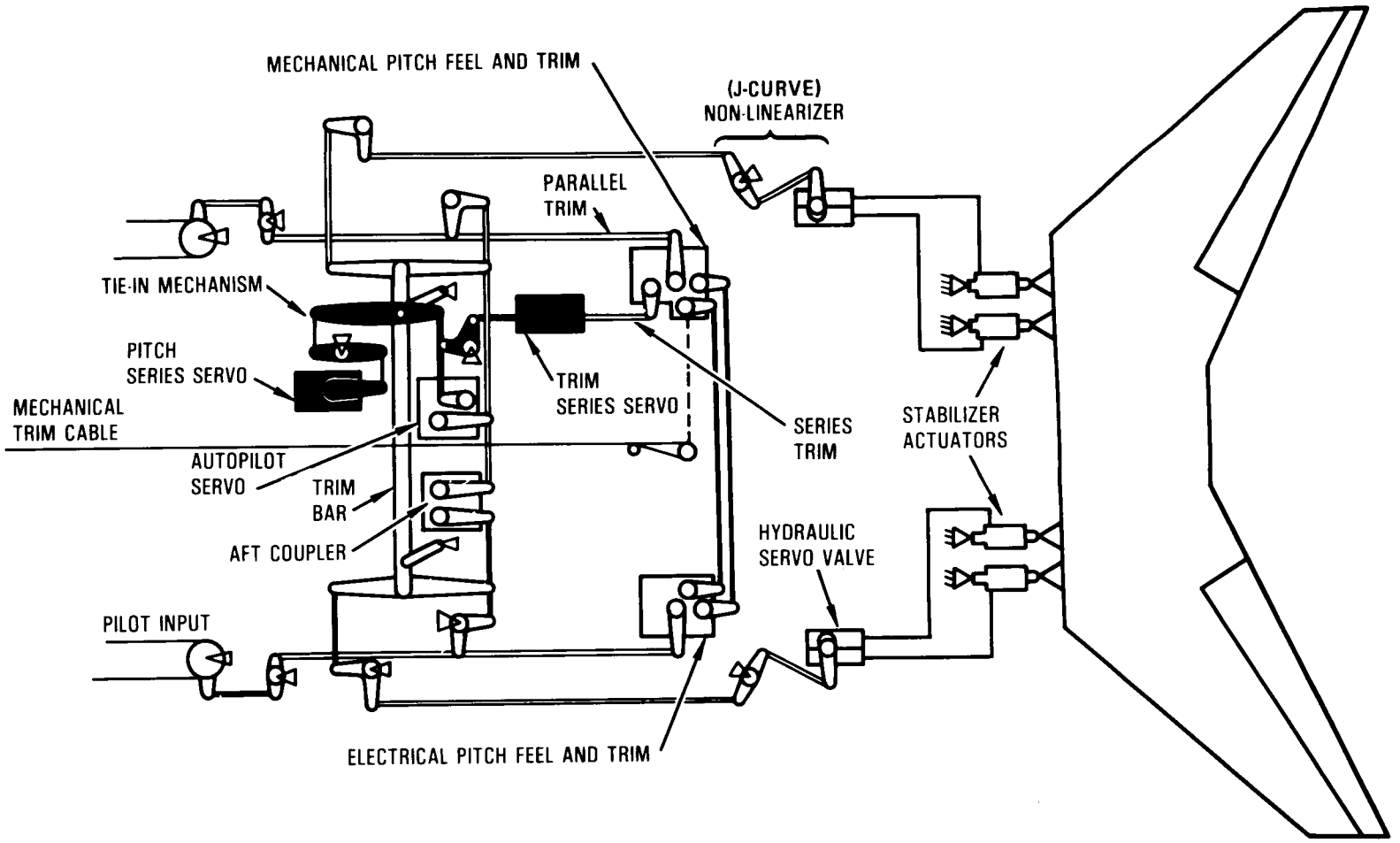

Figure 5. - Schematic of the L-1011 control system with the advanced PACS series servo.

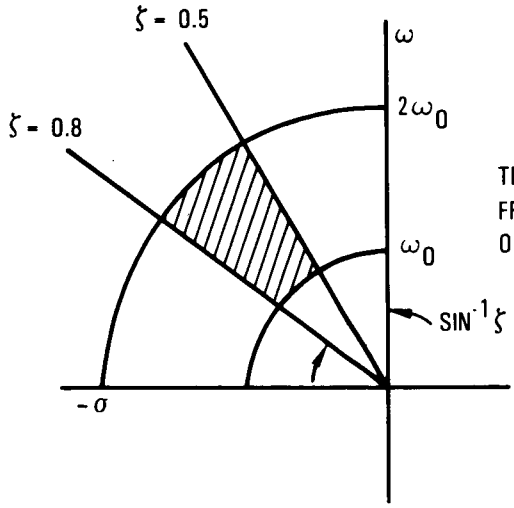

THE MINIMUM SHORT-PERIOD FREQUENCY $\omega_0 = \omega_{sp}$ @ 25% mac OPEN-LOOP CONDITION

A. SHORT PERIOD MODE

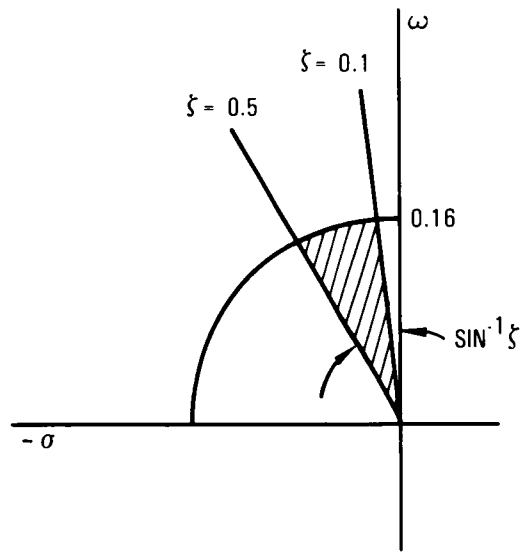

THE MINIMUM PHUGOID PERIOD = 40 sec

B. PHUGOID MODE

Figure 6. - PACS dynamic stability design objectives.

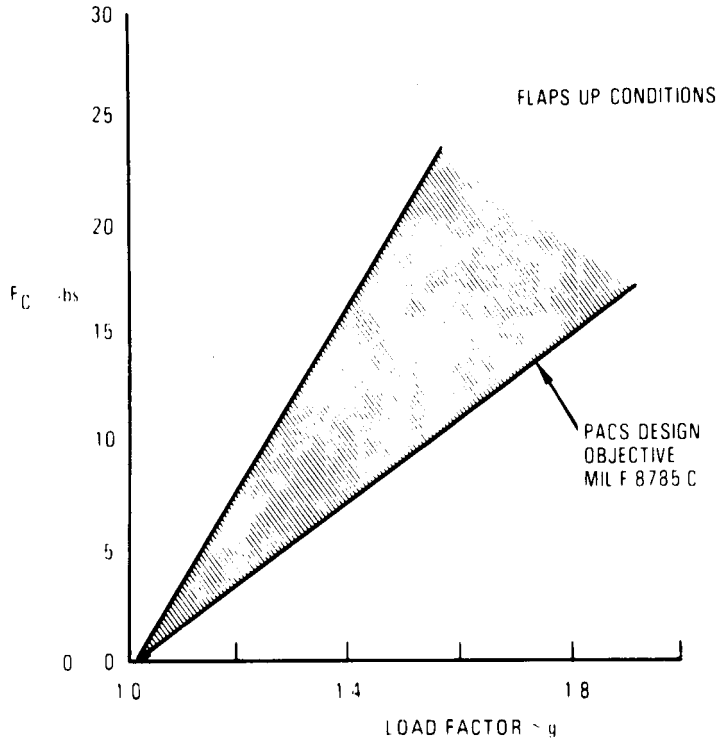

Figure 7.- PACS column force gradient design objective

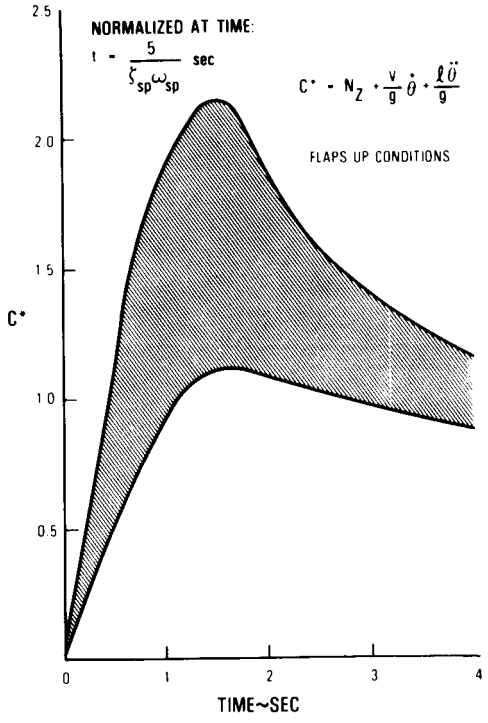

Figure 8.- Blended normal-acceleration/pitch-rate (C*) response objective

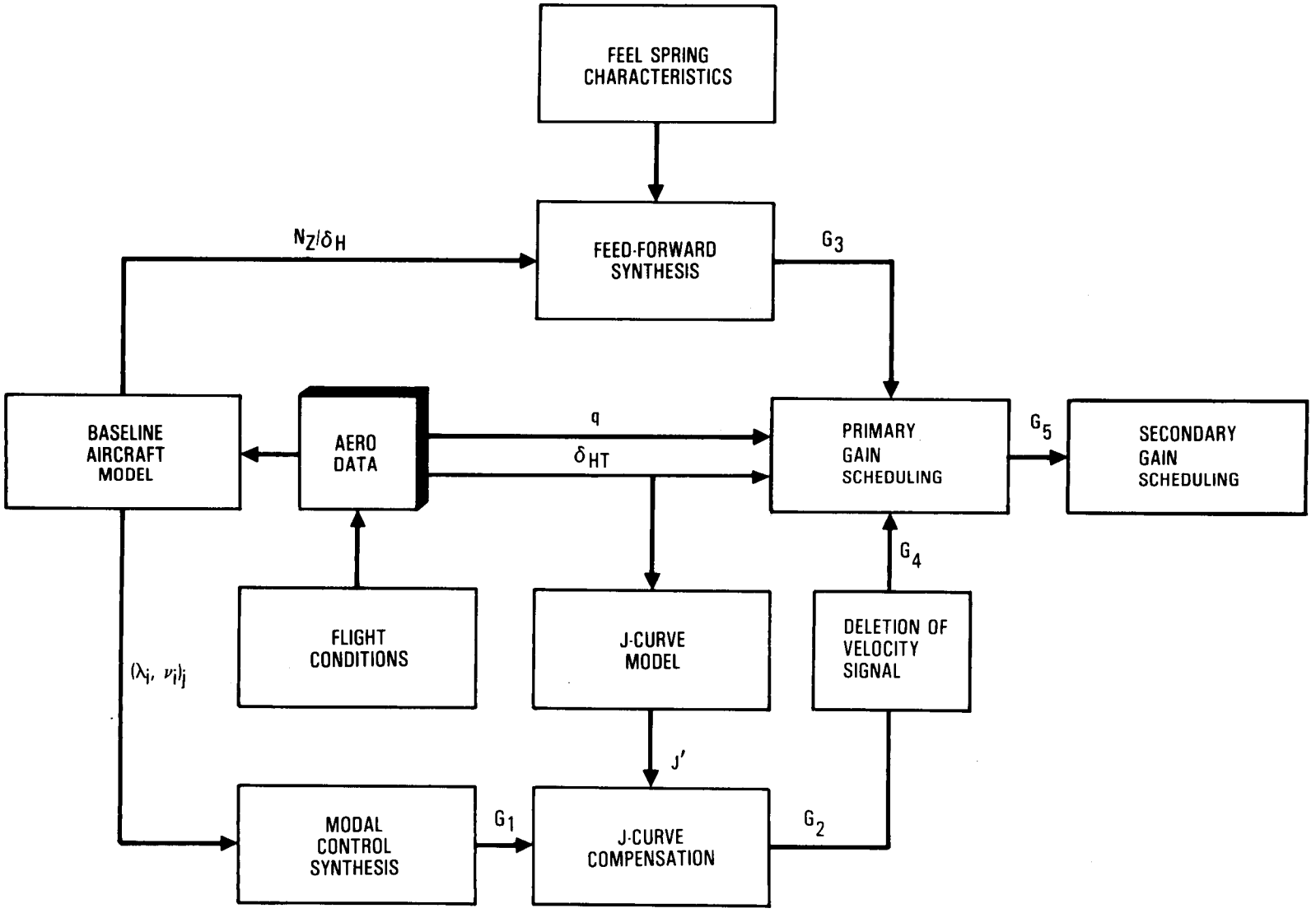

Figure 9. - Advanced PACS control law synthesis.

TABLE 2. - FLIGHT CONDITIONS USED FOR ADVANCED PACS CONTROL SYSTEM ANALYSIS

	c.g. ~ % mac										
FLIGHT CONDITION	FORWARD c.g. POSITION	MID c.g. POSITION	AFT c.g. POSITION	NEUTRAL STABILITY c.g. POSITION	NEGATIVE STABILITY c.g. POSITION	WEIGHT lbs	δ_F deg	h ft	V (KEAS/M)	ENGINE POWER	GEAR POSITION
	a	b	c	d	e						
1. TAKEOFF	19.6	25	32.2	37	–	422,000	26	S.L.	145/0.22	MTO	DOWN
2. TAKEOFF	13.8	25	35	42	–	305,000	26	S.L.	123/0.19	MTO	DOWN
3. CLIMB	–	25	32.2	37	50	422,000	0	10,000	274/0.5	MCT	UP
4. CLIMB	–	25	34.5	40.2	50	360,000	0	10,000	369/0.67	MCT	UP
5. CLIMB	–	25	35	42	50	305,000	0	10,000	369/0.67	MCT	UP
6. CRUISE	–	25	33.1	37.7	50	408,000	0	37,000	245/0.8	PLF	UP
7. CRUISE	–	25	33.1	37.7	50	408,000	0	37,000	254/0.83	PLF	UP
8. CRUISE	–	25	33.1	37.7	50	408,000	0	37,000	263/0.86	PLF	UP
9. CRUISE	–	25	33.1	37.7	50	408,000	0	37,000	276/0.9	PLF	IP
10. CRUISE	–	25	34.5	40.2	50	360,000	0	33,000	280/0.83	PLF	UP
11. CRUISE	–	25	35	42	50	285,000	0	33,000	290/0.86	PLF	UP
12. LANDING	16.4	25	34.5	40.3	–	358,000	42	S.L.	149/0.23	PLF	DOWN
13. LANDING	14.8	25	35	42	–	325,000	42	S.L.	142/0.21	PLF	DOWN
14. LANDING	12.0	25	35	42	–	265,000	42	S.L.	128/0.19	PLF	DOWN

- Modifying the feedback gains (G_1) to account for a nonlinear relationship between the L-1011 stabilizer rotation and control column displacement (J-curve). This is called J-curve compensation and provides a set of modified gains (G_2).

- Modifying the compensated gain matrix (G_2) to delete the requirement for a velocity sensor signal output. This provides the desired feedback gain matrix (G_4).

The baseline aircraft model shown in Figure 9 was the open loop state-space equation (Equation 1) given in Figure 10.

$$\{\dot{x}\} = [A]\{x\} + [B]\{u\} \qquad \text{(Eq. 1)}$$

The matrices are defined as follows.

A = Aerodynamic data

x = state-space vector

$\dot{x}$ = derivative of the state-space vector

u = input vector

B = input distribution matrix

Elements of the state-space vector and the input vector were:

$$\{x\} = \begin{bmatrix} \alpha \\ \dot{\theta} \\ \theta \\ u \\ N_{Z_F} \\ \dot{\theta}_F \\ \dot{\delta}_H \\ \delta_H \end{bmatrix}$$

α — angle of attack increment

$\dot{\theta}$ — pitch rate

θ — pitch attitude increment

u — normalized airspeed increment

N_{Z_F} — filtered normal acceleration increment

$\dot{\theta}_F$ — filtered pitch rate

$\dot{\delta}_H$ — horizontal stabilizer angular velocity

δ_H — horizontal stabilizer angular increment

$$\{u\} = \begin{bmatrix} \delta_{H_C} \\ \delta_{A_C} \end{bmatrix}$$

δ_{H_C} — horizontal stabilizer command signal

δ_{A_C} — Outboard aileron symmetrical deflection

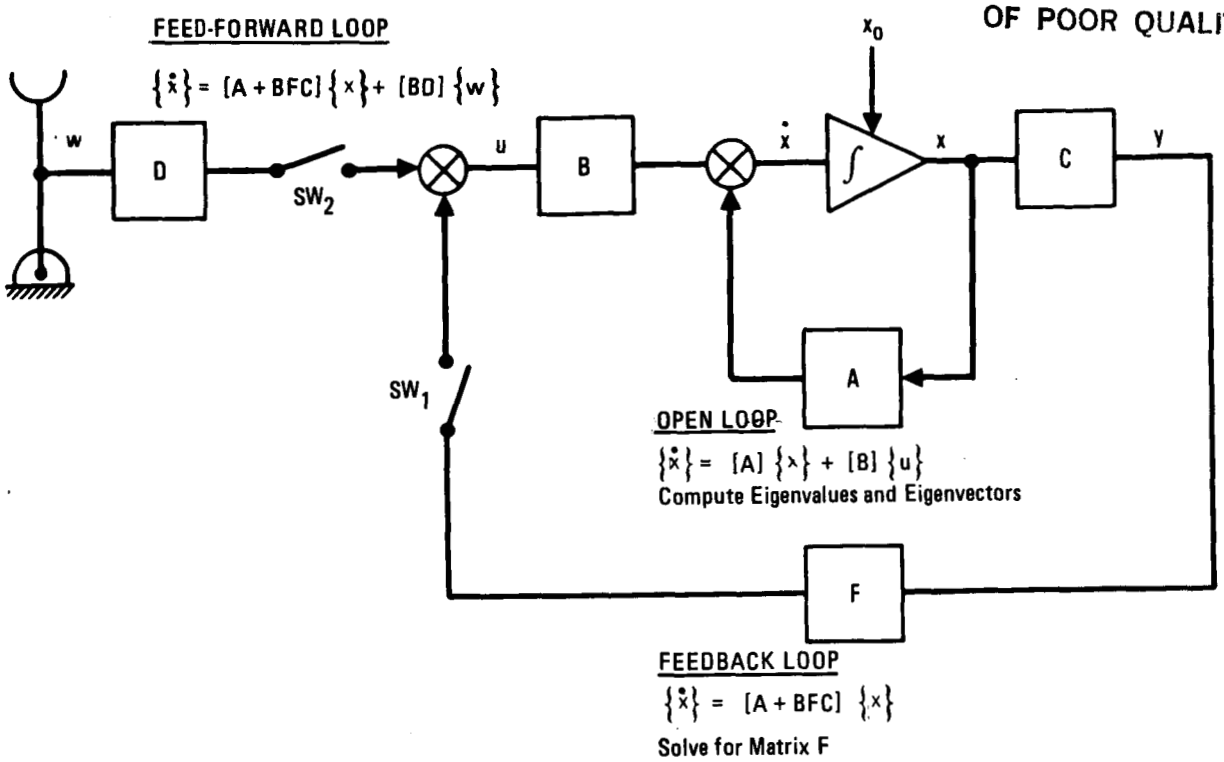

Figure 10. - Advanced PACS control math model in state-space form.

Equation 1 was used to obtain a set of eigenvalues and eigenvectors (λ_i, ν_i) at the 25 percent mac c.g. position for each of the 14 flight conditions listed in Table 2. This set of eigenvalues and eigenvectors, called the reference eigenstructure, provides values that are used for the modal control synthesis.

The modal control method of modern control theory was used to determine the feedback gain matrix G_1 (see Table 3). This method is superior to classical control theory because the gain for several feedback loops can be computed simultaneously instead of one at a time, and the pole placement in the complex plane is significantly simplified. Modal control synthesis was accomplished by the state-space feedback loop equation (Equation 2) given in Figure 10 with the switch (SW_1) closed.

$$\{\dot{x}\} = [A + BFC]\{x\} \qquad \text{(Eq. 2)}$$

Each element of Equation 2 is known except for the gain matrix F. Thus, the equation is solved for F to obtain the feedback gains for each flight case to provide the feedback gain matrix G_1. The elements of the state-space equation output distribution matrix (C) were arranged to provide the desired feedback loop signals: N_z and $\dot{\Theta}$ for control of the short-period mode, and u and Θ for control of the phugoid mode. Values of the elements for matrices A, B, and C are different for each c.g. location, whereas the reference set of eigenvalues (λ_i) and eigenvectors (ν_i) remain unchanged for each flight condition.

TABLE 3. - FEEDBACK GAIN MATRIX (G_1)

CASE	K_u	K_θ	K_{N_Z} deg/sec	$K_{\dot{\theta}}$ - sec
1A	0.0692	-0.116	-0.9855	-0.434
1B	0.104	-0.119	-1.8850	-0.444
1C	0.172	-0.134	-3.6039	-0.524
1D	0.227	-0.144	-5.0420	-0.584
2A	0.0718	-0.138	-1.4782	-0.595
2B	0.140	-0.144	-3.2143	-0.628
2C	0.257	-0.175	-6.3025	-0.796
2D	0.391	-0.209	-9.7403	-0.994
3B	0.0541	-0.0397	-0.1988	-0.130
3C	0.0747	-0.041	-0.2830	-0.155
3D	0.0863	-0.0402	-0.6188	-0.167
3E	0.142	-0.0446	-1.7991	-0.242
4B	0.00534	-0.011	0.1450	-0.0484
4C	0.0189	-0.0104	-0.1381	-0.0733
4D	0.0269	-0.00996	-0.3088	-0.0894
4E	0.043	-0.00962	-0.6303	-0.126
5B	0.00719	-0.0091	-0.1083	-0.0279
5C	0.0187	-0.00827	-0.1306	-0.0510
5D	0.0271	-0.00777	-0.2956	-0.0697
5E	0.0381	-0.00754	-0.5025	-0.0974
6B	0.0247	-0.0129	-0.04927	-0.162
6C	0.0126	-0.0127	0.09397	-0.154
6D	0.0241	-0.0125	-0.27674	-0.170
6E	0.0659	-0.0136	-1.4954	-0.252
7B	0.0612	-0.0144	2.1830	-0.118
7C	0.0873	-0.164	0.09397	-0.145
7D	0.0987	-0.0175	-0.25382	-0.159
7E	0.148	-0.024	-1.3997	-0.240
8B	-0.0037	-0.00949	0.43831	-0.108
8C	0.0180	-0.0104	0.01415	-0.125
8D	0.0351	-0.0112	-0.32429	-0.150
8E	0.0849	-0.0124	-1.3407	-0.217
9B	0.0356	-0.000699	-0.04956	-0.108
9C	0.0536	-0.00115	-0.50764	-0.141
9D	0.0674	-0.00146	-0.77922	-0.163
9E	0.101	-0.00205	-1.5871	-0.221
10B	-0.0378	-0.00881	0.28533	-0.130
10C	-0.0178	-0.00858	-0.20168	-0.158
10D	-0.00551	-0.00891	-0.52426	-0.136
10E	0.0201	-0.00906	-1.1345	-0.237
11B	0.0358	-0.00817	0.19022	-0.0769
11C	0.0548	-0.00843	-0.16902	-0.110
11D	0.0665	-0.00816	-0.43201	-0.133
11E	0.0834	-0.8821	-0.76203	-0.169
12A	0.0496	-0.0876	-0.64744	-0.393
12B	0.0957	-0.0938	-1.7704	-0.424
12C	0.170	-0.108	-3.5351	-0.501
12D	0.238	-0.124	-51.4516	-0.588
13A	0.0363	-0.0876	-0.82506	-0.420
13B	0.0876	-0.0945	-2.0798	-0.453
13C	0.162	-0.108	-3.8847	-0.528
13D	0.239	-0.124	-5.7869	-0.629
14A	0.0985	-0.114	-1.1860	-0.459
14B	0.157	-0.120	-25.9550	-0.478
14C	0.234	-0.136	-43.2583	-0.543
14D	0.319	-0.156	-6.1879	-0.634

The relationship between the L-1011 stabilizer rotation (δ_H) and the control column displacement (X_C) is a nonlinear function which is based on the stabilizer trim setting (δ_{HT}) as shown in Figure 11. Only the curves for δ_{HT} = 0 and δ_{HT} = -10 degrees are shown in the figure. However, a family of curves exist for points on the trim line. These curves are called the J-curve. Figure 9 shows that the stabilizer trim signal is obtained from the aerodynamic data and supplied to the J-curve model. This model is a set of equations that was curve fitted to the family of curves of Figure 11. The output of the J-curve model which was used for J-curve compensation was the J-curve derivative (J') corresponding to δ_{HT} for the specific flight case being evaluated. The slope of all members of the J-curve family is the same for any specified values of δ_{HT}.

The compensated feedback gain matrix (G_2) was determined by application of Equation 3.

$$[G_2] = [J']^{-1}[G_1] \qquad \text{(Eq. 3)}$$

J' is a diagonal matrix of the J-curve derivatives corresponding to the δ_{HT} for the 56 flight cases (Table 1).

Deletion of the velocity sensor is desirable because changes of trim conditions result in frequent velocity changes. Consequently a lag-lead circuit was devised to produce a signal component of derived incremental speed. Therefore, instead of using the velocity gain (K_u) and the pitch attitude gain (K_θ), a new set of gains were determined in terms of a combined pitch-attitude/velocity gain (K_3), a numerator time constant of the lag-lead circuit (τ_1), and a denominator time constant of the lag-lead circuit (τ_2). Thus the feedback gain matrix (G_4) is expressed in terms of the gains $K_{\dot{\theta}}$, K_{N_Z}, $1/\tau_2$, $\tau_2/\tau_1 - 1$, and $K_3\ \tau_1/\tau_2$.

2.2.2 Feed-forward loop.- The feed-forward loop synthesis considered switches SW_1 and SW_2 of Figure 9 to be closed. The control equation is expressed in terms of Equation 4.

$$\{\dot{x}\} = [A + BFC]\{x\} + [BD]\{w\} \qquad \text{(Eq. 4)}$$

Matrix D is the state-space feed-forward matrix and w is the pilot input vector. This equation was solved by taking the Laplace transform of Equation 4 and using Cramer's rule to obtain the force gradient (F_C/N_Z). Where F_C is the control column force and N_Z is the aircraft normal acceleration at some specified location.

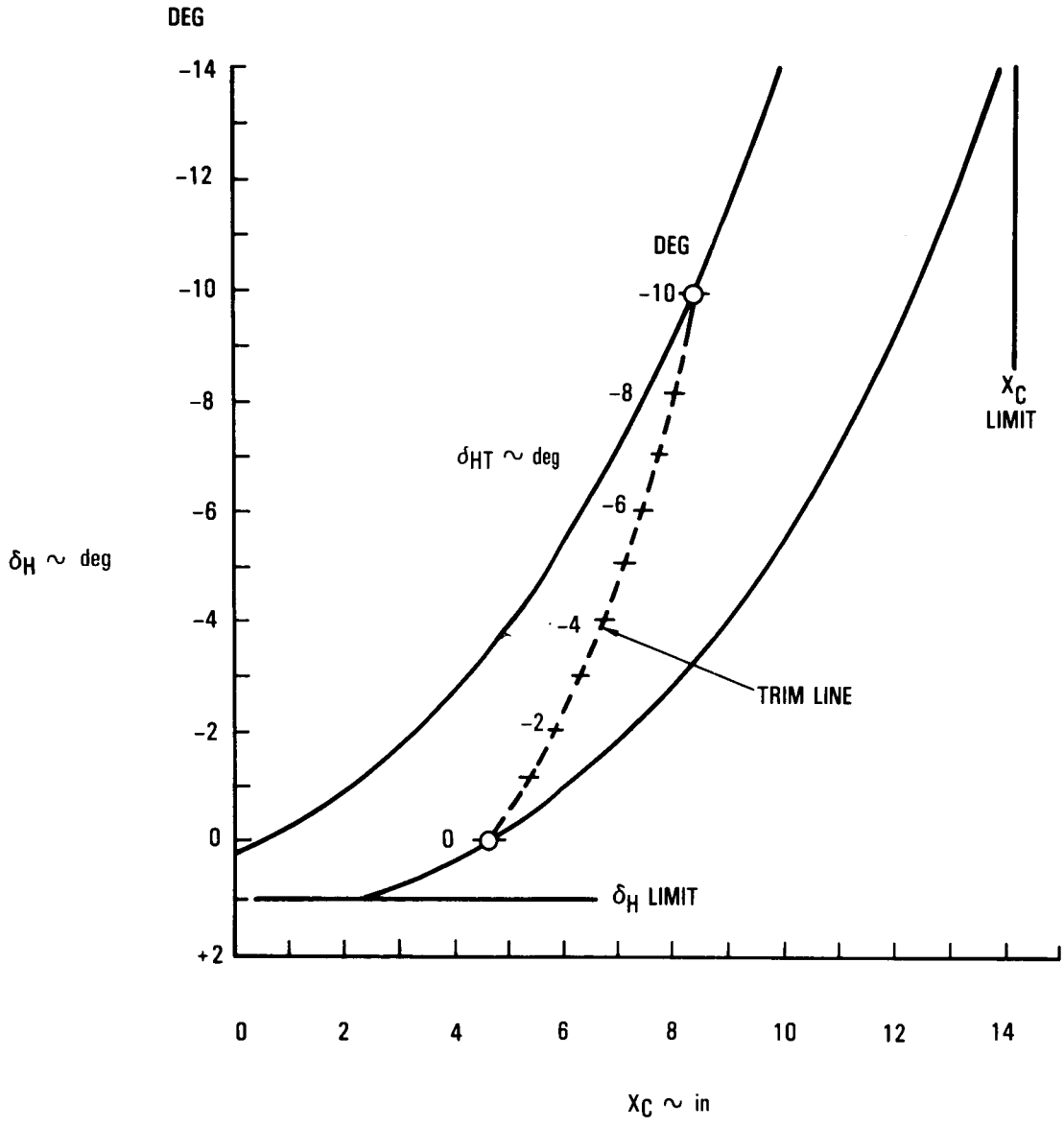

Figure 11. - L-1011 stabilizer rotation (δ_H) relative to control column displacement (X_C).

2.2.3 Primary gain scheduling.- Primary gain scheduling refers to a procedure which expresses the feedback matrix (G_4) and the feed-forward gain matrix (G_3) in the form of a second degree polynomial equation with parameters stabilizer trim (δ_{HT}) and dynamic pressure (q). Figure 9 shows that the δ_{HT} and q signals are provided from aerodynamic data for gain scheduling. The gain equation (Equation 5) is given below.

$$K = a + bq + cq^2 + d\delta_{HT} + e\delta_{HT}^2 \qquad \text{(Eq. 5)}$$

Symbols in the equation are:

K = feedback or feed-forward signal gains

a,b,c,d,e = Equation coefficients determined by using a least squares curve fit

Equation 5 was applied for the flap-up and flap-down cases to determine the equation coefficients for the feedback gains ($K_{\dot{\theta}}$, K_{N_Z}, $1/\tau_2$, τ_2/τ_1, $K_3\tau_1/\tau_2$) and the feed-forward gain (K_{FF}) which are given in Table 4. The flap-up flight conditions gain scheduling curves for the feedback gain ($K_{\dot{\theta}}$) and the feed-forward gain (K_{FF}) are plotted in Figures 12 and 13 respectively. The other feedback gains (K_{N_Z}, $1/\tau_2$, τ_2/τ_1, τ_1/τ_2) and the flap-down flight condition gains have a similar set of curves.

The primary gains such as those represented by the curves in Figures 12 and 13 are sufficient for gain scheduling of linear stability flight conditions. However, for nonlinear stability flight conditions, a secondary gain scheduling is required as described in the following section.

2.2.4 Secondary gain scheduling.- Secondary gain scheduling is required to compensate for:

- Pitch-up at high-Mach/high-g flight conditions
- Symmetric activity of the aileron active control system outboard ailerons

The pitch-up phenomena is caused by a loss of lift at the wing tips during the high-Mach/high-g flight conditions which causes the aerodynamic center of pressure (c.p.) to shift forward. Thus, the distance between the c.g. and the c.p. becomes less and the static stability margin is reduced in a manner similar to that when the c.p. is fixed and the c.g. is moved aft. Consequently, the gain scheduling curves already developed (e.g. Figures 12 and 13) can be used to stabilize the pitch-up conditions.

TABLE 4. - PACS GAIN SCHEDULE EQUATION COEFFICIENTS

FLAP SETTING	COEF.	$K_{\dot{\theta}}$ ~ sec	K_{N_Z} ~ deg/g	$1/\tau_2$ - sec^{-1}	τ_2/τ_1 - 1	$K_3\,\tau_1/\tau_2$	K_{FF} ~ in/lb
FLAPS-UP	a	-1.4295	9.7718	2.2322×10^{-2}	-2.9433 x 10	-1.4028×10^{-1}	2.1328×10^{-2}
	b	1.5023×10^{-3}	8.96×10^{-3}	-2.8474×10^{-5}	2.9511×10^{-1}	1.5431×10^{-4}	2.0571×10^{-4}
	c	0	0	0	-4.1698×10^{-4}	0	-4.0915×10^{-7}
	d	-5.0386×10^{-1}	4.5098	0	4.2547	-4.2834×10^{-2}	2.6975×10^{-2}
	e	-7.6620×10^{-2}	6.0459×10^{-1}	0	0	-7.4588×10^{-3}	3.8428×10^{-3}
FLAPS DOWN	a	-3.6149	36.2224	8.7222×10^{-2}	-1.5771	-1.0483	3.2829×10^{-1}
	b	1.1658×10^{-2}	9.9013×10^{-2}	-4.7143×10^{-4}	1.8067×10^{-1}	4.0908×10^{-3}	2.4014×10^{-3}
	c	0	0	0	-1.4232×10^{-3}	0	-3.5719×10^{-5}
	d	-6.0629×10^{-1}	7.0302	0	3.4827×10^{-1}	-1.5772×10^{-1}	6.8201×10^{-2}
	e	-3.9313×10^{-2}	4.3358×10^{-1}	0	0	-9.7027×10^{-3}	4.0296×10^{-3}

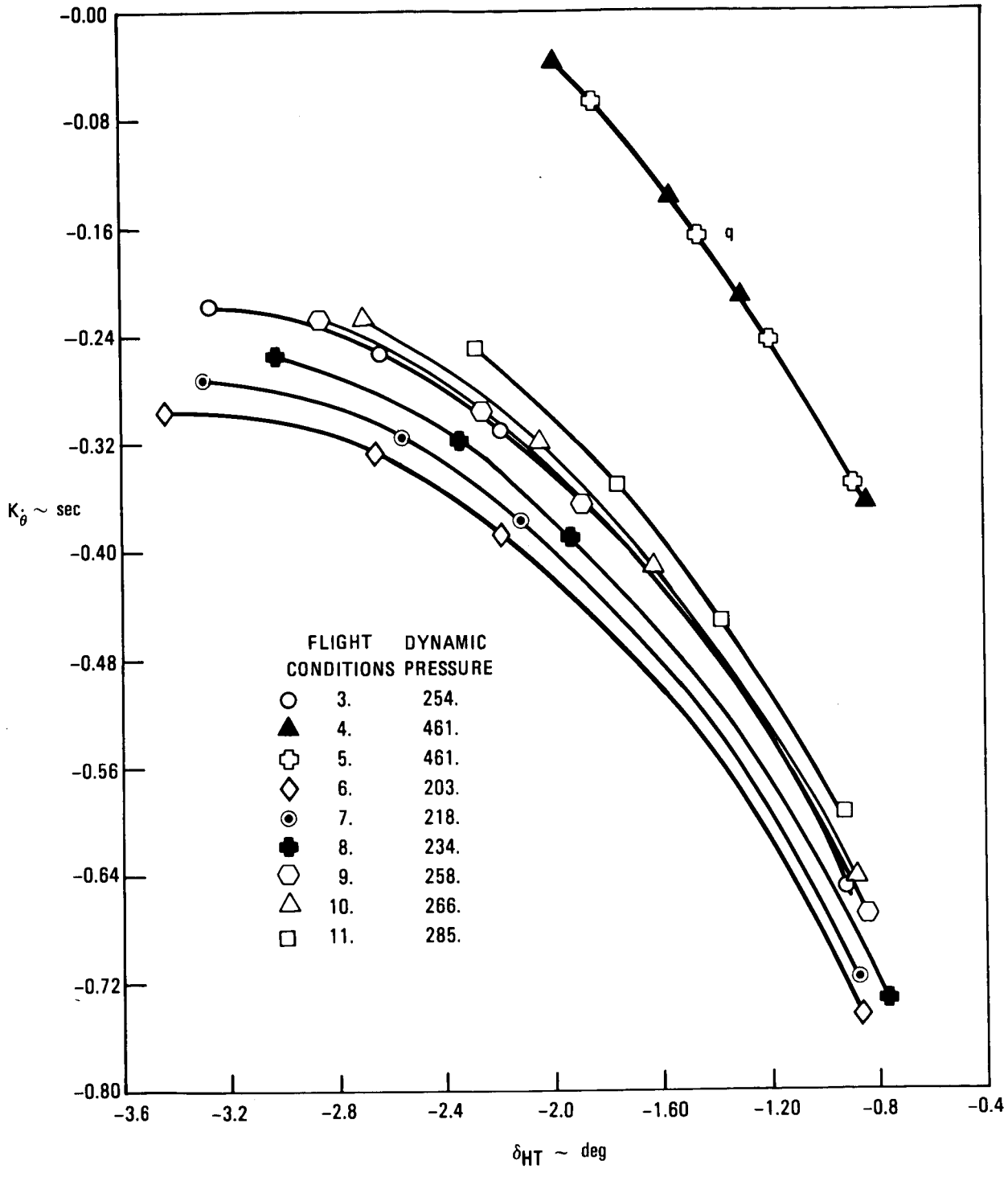

Figure 12. - Scheduled pitch rate feedback gain curves, flaps-up conditions.

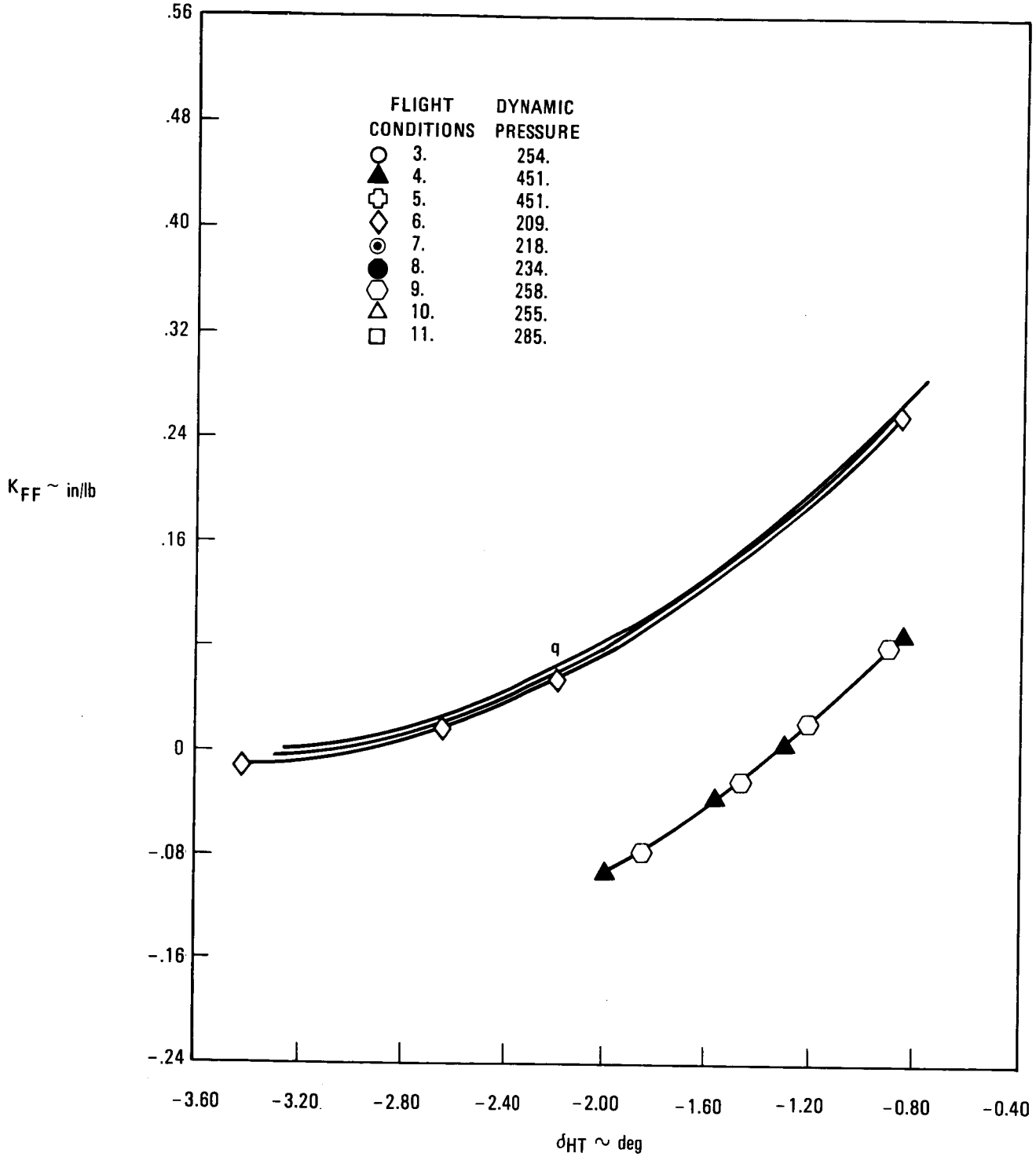

Figure 13. - Scheduled feed-forward gain curves flaps-up conditions.

The value of δ_{HT} is incremented by the secondary gain controller (Figure 14) to provide a modified value δ_{HT}* (see Figure 4).

Signals required to provide the correct δ_{HT}* value are angle of attack (α), bank angle (ϕ), and Mach number (M) as shown in Figure 14. The modified value δ_{HT}* changes the feedback gains to provide the increased control command for the horizontal stabilizer and changes the feed-forward gains to provide the desired column force gradients.

The AACS operates the outboard ailerons in a symmetric mode in response to normal acceleration of the aircraft c.g. and wing tips. This symmetric mode produces a c.p. shift that is equivalent to an aft c.g. shift of about five percent mac. The change in pitching moment can be corrected in the same way as for the pitch-up condition. This is accomplished by switch SW_1 in Figure 14. Also, a switch SW_2 provides for flap-up and flap-down gain changes. Switch SW_1 is automatically closed when the AACS is engaged and SW_2 is automatically operated to correspond to the flap setting.

2.2.5 Advanced PACS control law.- The advanced PACS control law block diagram is given in Figure 15. The diagram is considered to be divided into three parts for the purpose of discussion.

- Control column and actuator system: control column, column trim, series servos, J-curve, stabilizer trim, and power actuator
- Feedback loops: pitch rate ($\dot{\theta}$), normal acceleration (N_Z), and pitch attitude (θ)
- Feed-forward loop: column force (F_C)

The control column and actuator system is considered to start with the control column displacement (X_C) and the control column trim (X_T). These inputs are summed with the series servo outputs (X_S). The nonlinearizer (see Figure 5) represented by the J-curve (J) provides the J-curve compensation. The stabilizer trim (δ_{HT}) is then subtracted to provide the stabilizer servo command signal (δ_{HC}). The stabilizer servo controls the hydraulic flow to the stabilizer power actuators to provide the desired stabilizer angle (δ_H). The power actuator lag characteristics are shown in the figure to be $1/(\tau_P s+1)$. Where τ_P is the power actuator time constant and s is the Laplace Transform parameter.

The feedback loop uses the $\dot{\theta}$ and N_Z feedback signals for control of the short-period modes. These signals are filtered thru the first order low-pass filters, $1/(\tau_Z s + 1)$ and $1/(\tau_{\dot{\theta}} s + 1)$, shown in Figure 15. The filter time constants τ_Z and $\tau_{\dot{\theta}}$ are equal to 0.03 seconds. The filtered signals $\dot{\theta}_F$ and N_{Z_F} are subjected to the scheduled gains $K_{\dot{\theta}}$ and K_{N_Z} respectively. A normalizing constant $1/K_c$ is used in each feedback loop signal so that gain schedules thru the J-curves provide a δ_{HT} value of 10 degrees to produce a

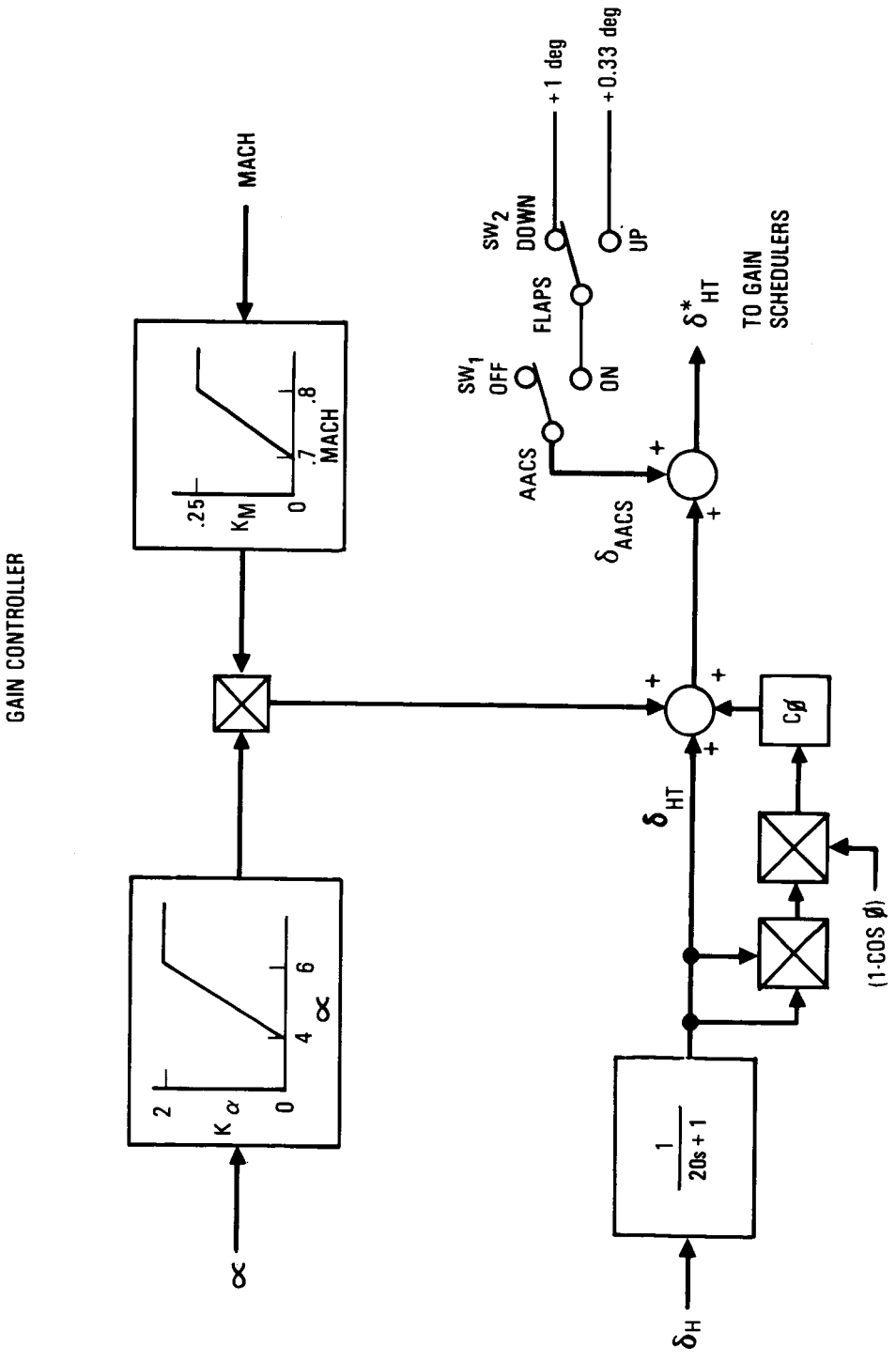

Figure 14. - Advanced PACS secondary gain controller.

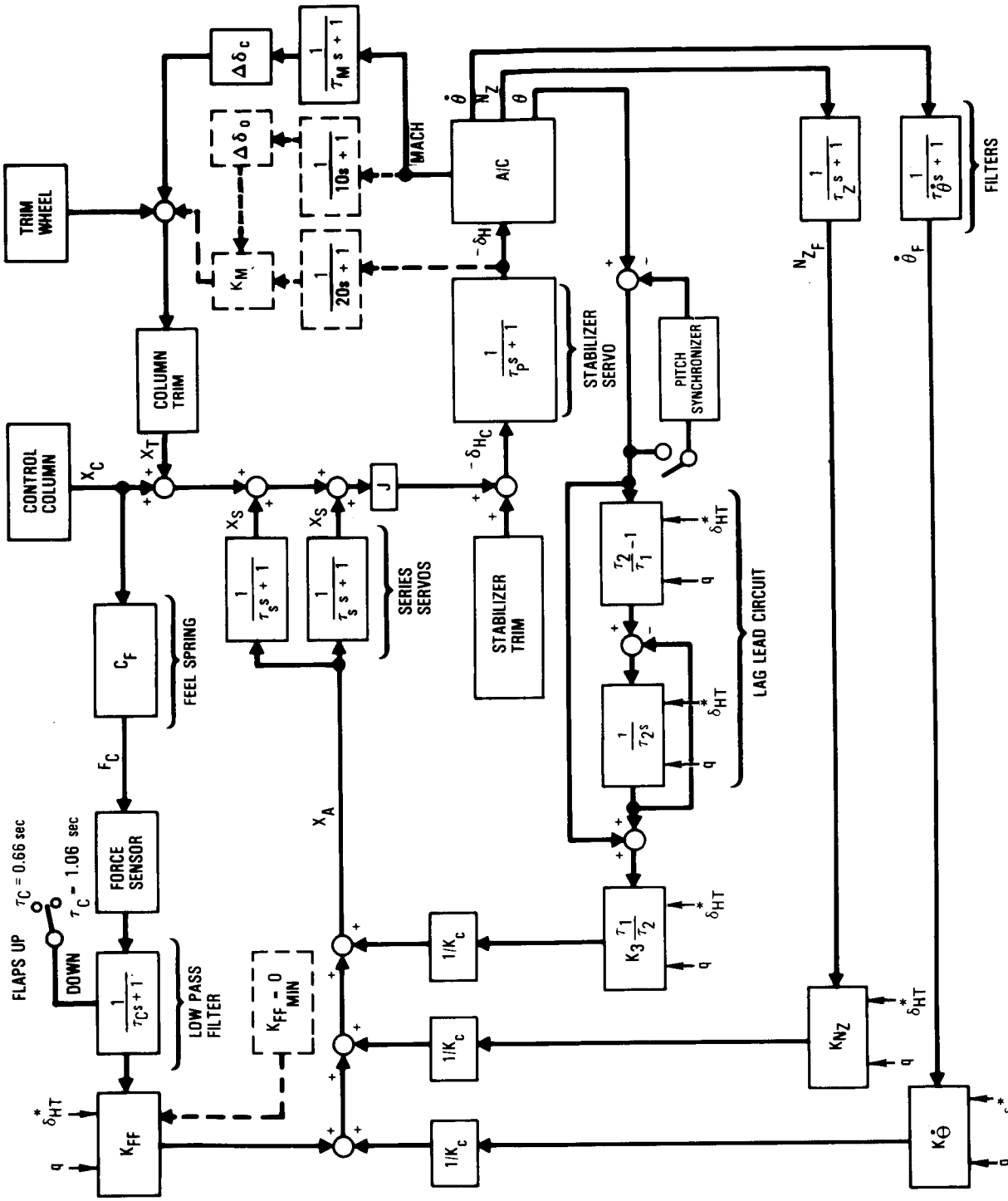

Figure 15. - Advanced PACS control law block diagram.

signal value of 1. The θ feedback signal is used to control the phugoid mode. This signal is processed through a pitch synchronizer, a lag-lead, circuit, and a gain amplifier. The pitch synchronizer suppresses the attitude hold during maneuvers and sets a new attitude reference at the synchronizer output when a control column force is applied. The lag-lead circuit eliminates the need for a velocity signal that would be required for phugoid mode control. Thus, the resulting set of gains to be scheduled are: $(\tau_2/\tau_1 - 1)$, $1/\tau_2$, and $K_3(\tau_1/\tau_2)$.

The feed-forward loop is used to provide the desired control column force gradients. The feel-spring (C_F) converts the control column displacement (X_C) to column force (F_C). The force sensor converts F_C to an electrical signal. A flaps-up/flaps-down bias signal switch the low-pass filter time constant (τ_C) from 0.66 sec for flaps-up to 1.06 sec for flaps-down. These time constants are related to the short-period mode of the baseline aircraft. The signal is then passed through the scheduled feed-forward gain (K_{FF}) and is summed with the feedback signals to provide the series servo input signal (X_A).

The dashed lines in Figure 15 represent a Mach compensation circuit and a feed-forward gain lower limit ($K_{FF} = 0$) which was added to provide the required speed stability (see Section 2.3.3) that was not accounted for in the initial control law development. The Mach compensation circuit consists of two circuits that operate through the Mach trim system. The Mach trim compensation $\Delta\delta_c$ and corresponding filter was part of the baseline aircraft control system. The Mach trim servo offset schedule ($\Delta\delta_o$) and the loop gain schedule (K_M) provide the desired control column force gradient for speed stability of the PACS configured Aircraft. The stabilizer gain filter has a 20 second time constant and the offset schedule filter has a 10 second time constant to limit series servo offset gain overshoot.

2.3 FLYING QUALITY ANALYSIS

The validity of the control law was evaluated for the flight conditions that were to be used for the piloted flight simulation test (Table 5). The analysis included dynamic stability, maneuver stability, speed stability, and trimmability.

2.3.1 Dynamic stability.- Dynamic stability analysis included linear analysis and nonlinear analysis applications.

The linear analysis was performed to show that the characteristic roots of the control system met the design objectives of Figure 6. This was accomplished by plotting the short-period and phugoid mode root loci of each flight condition for c.g. locations from 25 to 50 percent mac in the complex(s) plane.

TABLE 5. - PILOTED FLIGHT SIMULATION TEST CONDITIONS

Flight Condition	Weight 1000 lbs	c.g. % mac	Altitude 1000 ft	V KEAS
7. Cruise $W/\delta = 1.9 \times 10^6$ lbs	408	25 to 50	37	254 (M = 0.83)
10. Cruise $W/\delta = 1.4 \times 10^6$ lbs	360	25 to 50	33	260 (M = 0.83)
15. Cruise $W/\delta = 1.6 \times 10^6$ lbs	360	25 to 50	36	280 (M = 0.83)
16. M_{mo}/V_{mo}	350	25 to 50	25	357
17. Holding	335	25 to 50	10	250
18. Landing (δ_F = 33 deg)	330	25 to 50	2	135 (1.3 V_s)
19. Takeoff (δ_F = 26 deg)	380	25 to 50	2	137 (1.2 V_s)

The nonlinear analysis was performed to determine time histories of the longitudinal dynamic response for control column step inputs and for discrete vertical gusts. Figure 16 shows the aircraft response for angle of attack, pitch rate, and load factor with the PACS on and off for Flight Condition 7 (Table 5) with the c.g. at 50 percent mac. The baseline aircraft diverges quickly from its trim condition for any constant force input until it reaches a region of increased stability at high angle of attack. Engagement of the PACS reduces the angle of attack and load factor excursions significantly. Figure 17 gives a comparison of the aircraft response with the PACS off and on for a discrete severe vertical gust with a peak of -54 ft/sec. This gust is representative of a severe disturbance for a heavy thunderstorm. For this severe disturbance the baseline airplane with c.g. at 25 percent mac will return to its initial trim condition. If the c.g. is aft of 25 percent mac, the aircraft diverges from its trim condition and seeks a new equilibrium at high angle of attack. The PACS configured aircraft had well-behaved and stable response characteristics for all of the c.g. positions from 25 to 50 percent mac.

Figure 18 shows that the blended normal-acceleration/pitch rate response (C*) for flight condition 7 with the c.g. at 25 percent mac was in compliance with the design objective (Figure 8).

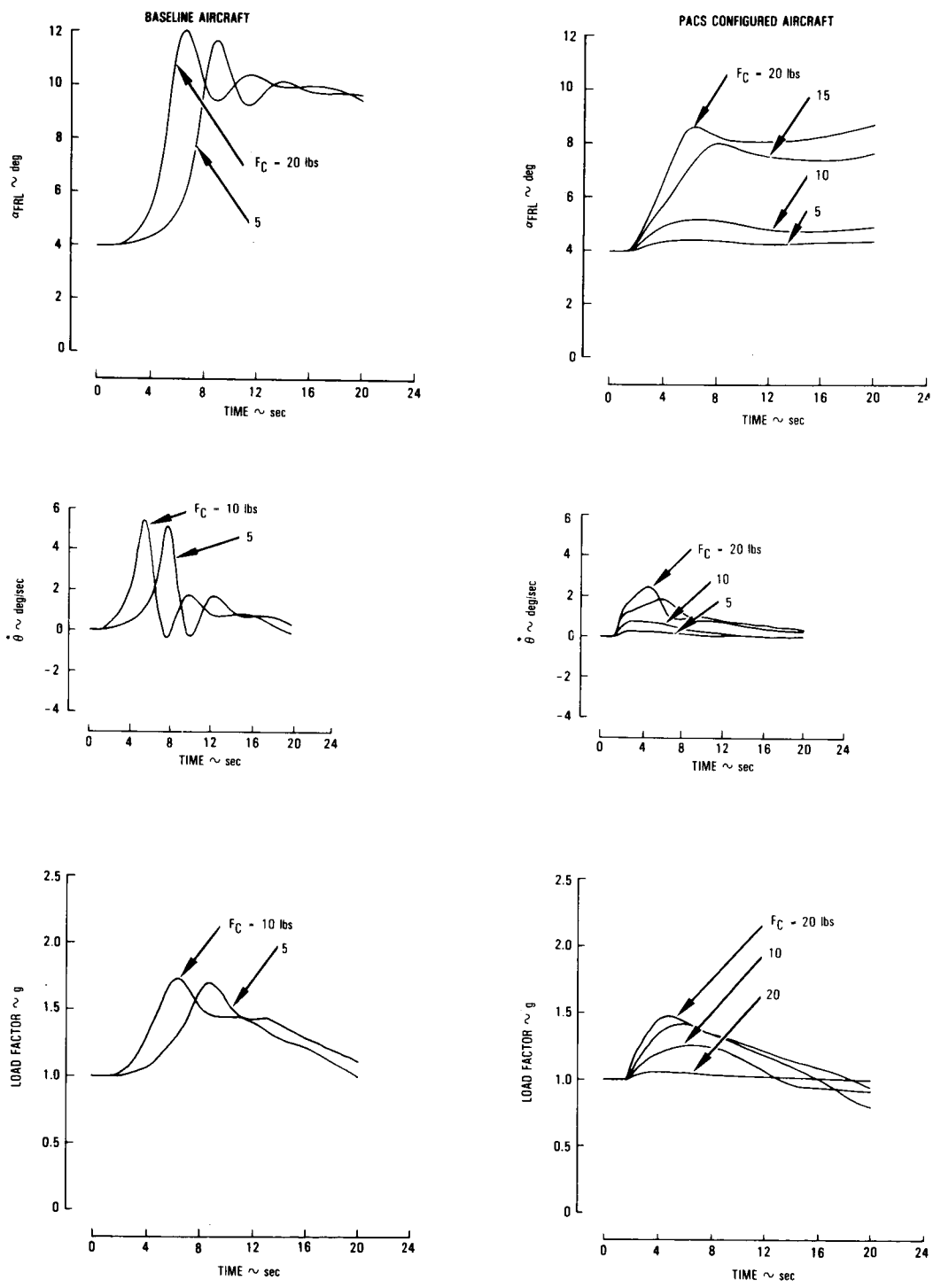

Figure 16. - Comparison of aircraft response with and without PACS engaged for various levels of control column step inputs.

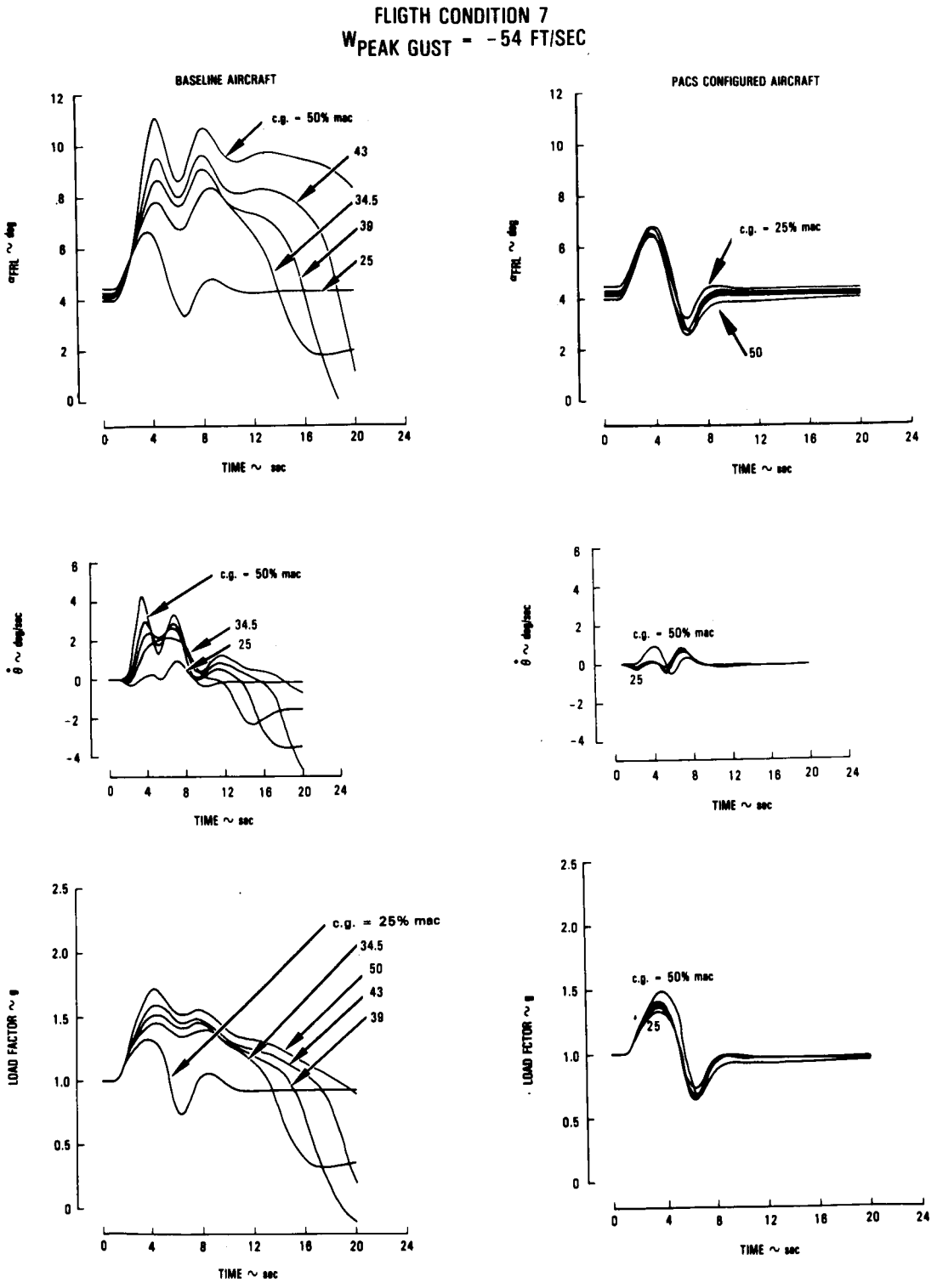

Figure 17. - Comparison of aircraft response with and without PACS engaged for a severe vertical gust.

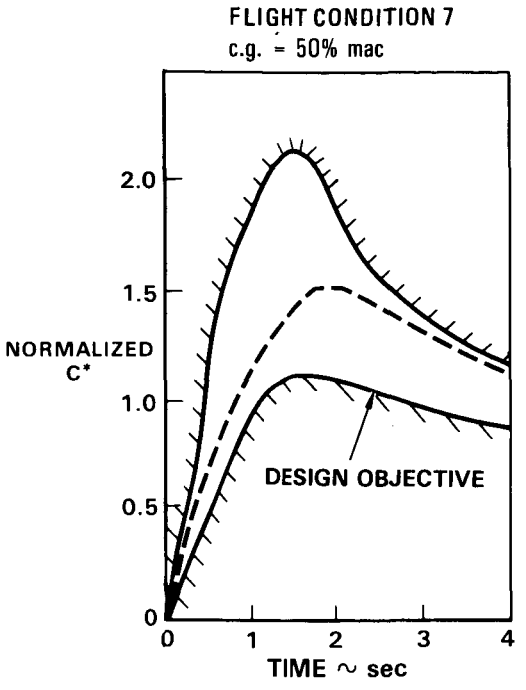

Figure 18. - Blended normal-acceleration/ pitch-rate response.

2.3.2 Maneuver stability.- The maneuver stability analysis was performed to determine the control column force gradient as a function of load factor. The baseline aircraft maneuver stability control column characteristics for cruise are shown in Figure 19. These data show that the force gradients for each c.g. location does not comply with the MIL-F-8785C criteria in the nonlinear stability flight condition range.

Engagement of the PACS improved the column force gradients significantly as shown in Figure 20. This improvement complies with the design objective except at high load factors and is primarily due to the secondary gain scheduling. To evaluate the secondary gain schedule, the six PACS operating configurations listed in Table 6 were analyzed. Configuration number two (the PACS with full gain) was shown to provide the best control column gradient.

2.3.3 Speed stability.- The speed stability analysis determines the control column force required to maintain the aircraft at speeds different from the trim speed. FAR Part 25 requirements were used as the speed stability criteria. FAR Part 25 defines satisfactory column force characteristics as follows.

- A pull force shall be required to maintain speed below trim speed and a push force shall be required to maintain speed above trim speed.

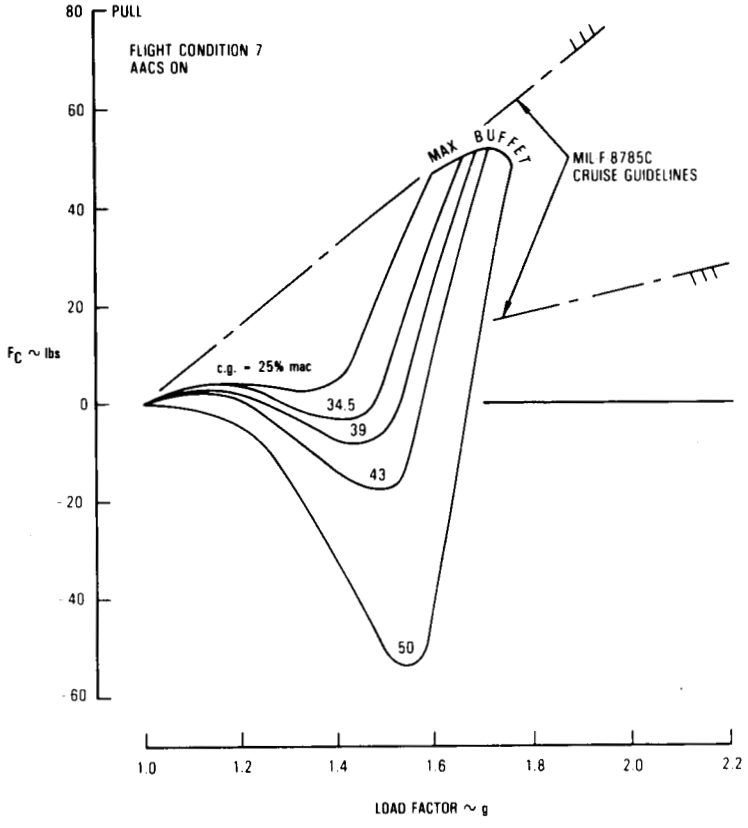

Figure 19. - Baseline aircraft maneuver stability column force gradients, cruise.

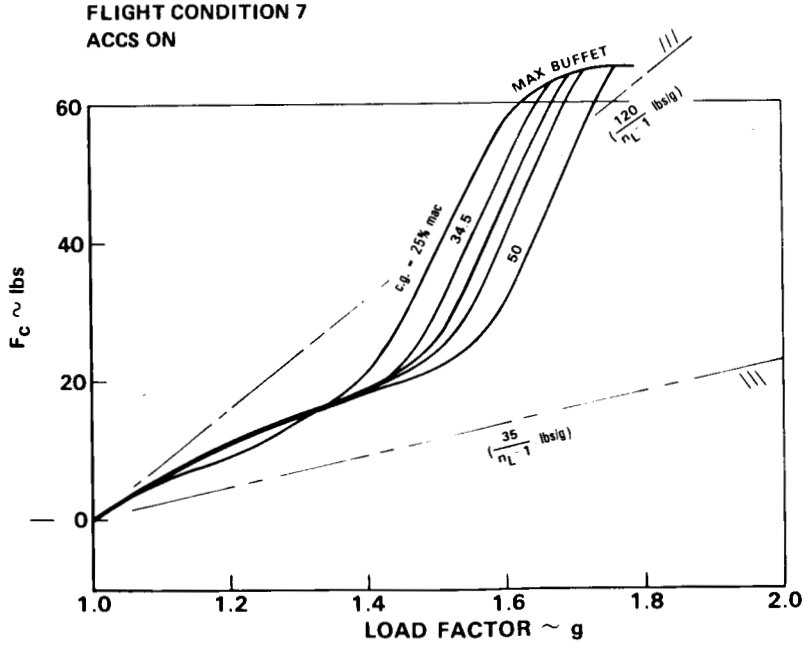

Figure 20. - PACS configured aircraft maneuver stability column force gradients, cruise.

TABLE 6. - PACS OPERATING CONFIGURATIONS EVALUATED

GAINS / PACS CONFIGURATION	FEEDBACK	FEED-FORWARD	AUGMENTED GAIN SCHEDULE	
			BANK ANGLE	ANGLE OF ATTACK
1. BASELINE AIRCRAFT	$K_{\dot{\theta}}, K_{\theta}, K_{u}, K_{N_Z}$	–	–	–
2. PACS/FULL GAIN	$K_{\dot{\theta}}, K_{\theta}, K_{N_Z}$	K_{FF}	K_{ϕ}	K_{α}
3. PACS/PARTIAL GAIN	$K_{\dot{\theta}}, K_{\theta}, K_{N_Z}$	K_{FF}	–	K_{α}
4. PACS/NO FEED-FORWARD	$K_{\dot{\theta}}, K_{\theta}, K_{N_Z}$	–	–	K_{α}
5. PACS/ONE-G GAIN	$K_{\dot{\theta}}, K_{\theta}, K_{N_Z}$ = CONST	K_{FF} = CONST	K_{ϕ} = CONST	K_{α} = CONST
6. PACS/QUASI-STEADY GAIN	$K_{\dot{\theta}}, K_{\theta}, K_{N_Z}$ = CONST	K_{FF} = CONST	K_{ϕ} = CONST	K_{α}

- Stick forces shall vary monotonically with speed.
- The average stick force gradient shall be at least -1 lb per six KEAS increase throughout the speed range.

Speed stability had not been included in the design criteria for control law development. Consequently, the speed stability analysis showed an abrupt column force reversal for the takeoff condition with c.g. at 25 percent mac and unstable column force gradients for the 50 percent c.g. location. These problems were corrected by limiting the lower bound of the feed-forward gain (K_{FF}) to zero and by adding a Mach compensation circuit that operates through the Mach trim system (Figure 15). The speed stability column forces for the PACS with Mach compensation are shown in Figure 21 for c.g. positions from 25 percent to 50 percent mac. As shown in the figure, the speed stability satisfies the FAR Part 25 criteria.

2.3.4 Trimmability.- This analysis was performed to determine changes of the baseline aircraft control system that were required for the advanced PACS configured aircraft. Control system characteristics that were evaluated included: stabilizer/elevator deflection range, trim servo range, elevator versus stabilizer gearing relationship, control column limits, and pitch feel-spring rate. The control system design criteria were:

- Capability must be provided to trim the aircraft for all flight conditions

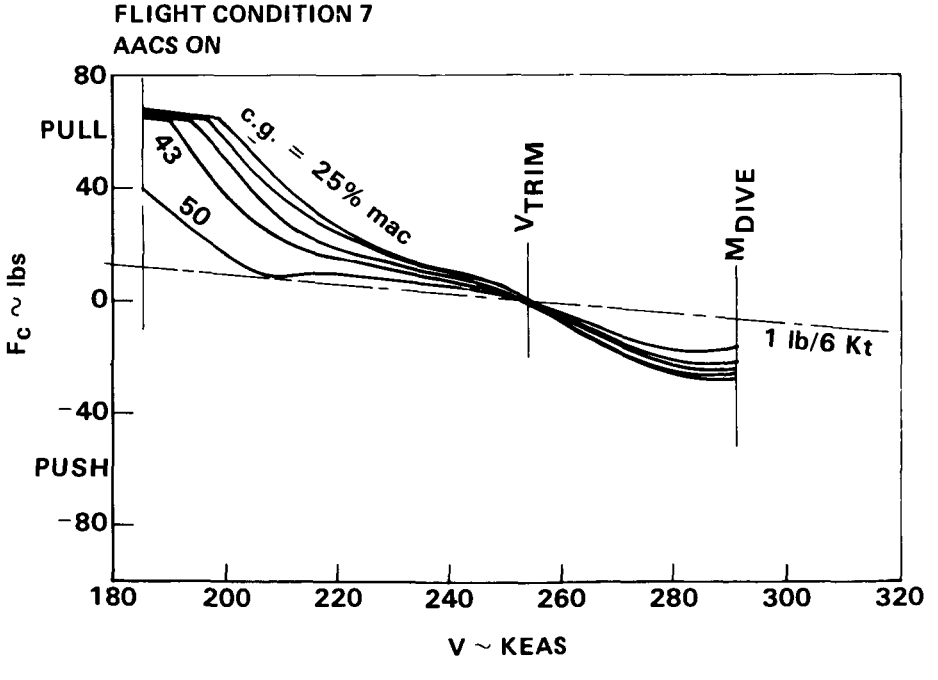

Figure 21. - Speed stability column forces, cruise.

- Sufficient control power must be provided to give a minimum pitch angular acceleration of -5.73 deg/sec^2 for stall recovery from any flight condition

- Control power must be provided to recover from maneuvers in high angle-of-attack regions.

The baseline L-1011 c.g. range is 12 to 35 percent mac. The corresponding stabilizer/elevator deflection range is from -14 deg/-25 deg nose-up to +1 deg/0 deg nose-down. The stabilizer deflection trim range is -10 deg to 0 deg. The advanced PACS configured c.g. range is 25 to 50 percent mac. Analysis showed that the corresponding stabilizer/elevator deflection range should be from -14 deg/-20 deg nose-up to +4 deg/+5 deg nose-down, and the trim range should be -10 deg to +1 deg.

Thus, modifications of the stabilizer/elevator gearing curve, the J-curve, the trim servo, and the feel-spring rate would be required for the L-1011 in order to flight test an advanced PACS to a three percent negative stability margin. This three percent negative stability margin represents the aft c.g. limits for which the L-1011 can be tested without significant modifications.

2.4 Piloted Flight Simulation Test

The advanced PACS piloted flight simulation test was performed to identify pilot/control interface problems and to evaluate flying qualities of the aircraft. The test was performed at the NASA Langley Flight Simulation Facilities. Setup of the simulator included a check of the simulation computer program, motion system interface, cockpit controls, and instrumentation. Two Lockheed and three NASA pilots performed the flight simulation tests.

2.4.1 Flight Simulator.- The NASA flight simulator is a visual motion simulator with a two-man cockpit mounted on a six degree-of-freedom synergistic motion base. A collimated visual display provides a 60 degrees out-the-window color display which was activated during the landing approach task.

2.4.2 Simulation Computer Program.- The simulation mathematical model represents the L-1011 S/N 1001 Aircraft. Engine characteristics were represented by the installed thrust for three Rolls Royce R.B.211-22B high-bypass ratio turbofan engines.

2.4.3 Simulation Test Conditions.- The piloted flight simulation test conditions are listed in Table 5 and designated in Figure 22. The simulation tests were performed for calm air and moderate turbulence atmospheric conditions. Evaluation tasks performed for the different flight conditions are listed in Table 7.

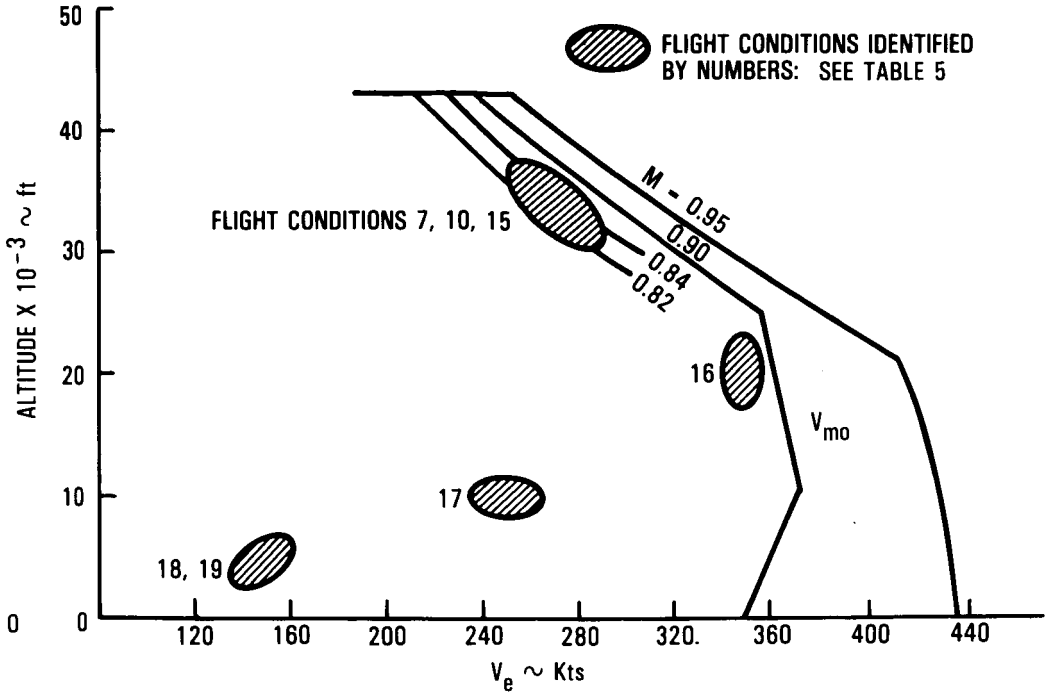

Figure 22. - Piloted flight simulation test conditions.

TABLE 7. - PILOTED FLIGHT SIMULATION EVALUATION TASKS

Evaluation Task	Flight Conditions				
	Cruise	Max. Oper. Speed	Landing	Holding	Takeoff
Wind-up turns	X	X	X		
S-pattern turns	X				
Airline operational turns	X	X		X	
Trimmability	X	X			
Pitch attitude change	X				
Power effects	X				
Emergency descent	X				
Short-period mode stability	X				
Phugoid mode stability	X				
ILS approach			X		
Heading change					X

2.4.4 Simulation Test Results.- The pilot used the Cooper-Harper rating scale (NASA TND-5163) given in Figure 23 to evaluate the aircraft flying qualities with the PACS on and off. Ratings for each pilot were plotted as shown in Figure 24. A summary of the test results is shown in Figure 25. With the PACS off the pilot ratings became unacceptable (Cooper-Harper rating of 6.5) when the c.g. was near the neutral point. However, engagement of the advanced PACS resulted in good handling qualities over the entire c.g. range of from 25 to 60 percent mac.

2.5 PACS System Architecture

This section shows how the control laws were mechanized to provide an advanced PACS which is suitable for performing flight tests with the Lockheed house L-1011 (S/N1001). Aft c.g. location constraints do not permit flight at negative static stability margins greater than three percent mac.

The advanced PACS interface block diagram is shown in Figure 26. The controller input signals from each sensor element are shown on the left side of the figure along with the electrical power. Output signals to the series servo channels and failure signals to the Flight Control Electronic System (FCES) panel are shown on the right side of the illustration.

Safety provisions criteria were as follows. Single failures are bound to occur and it is impossible to predict exactly when they will happen. Therefore, the design aim is to incorporate safety provisions that will protect the system against critical effects for any single failure. Also, the flight crew needs to be warned of any failure, critical or not, so that exposure time for build up of possible hazardous multiple failures and the probability of potential hazardous single failures are acceptably remote. The redundancy of the advanced PACS components to comply with this criteria is shown in Figure 27.

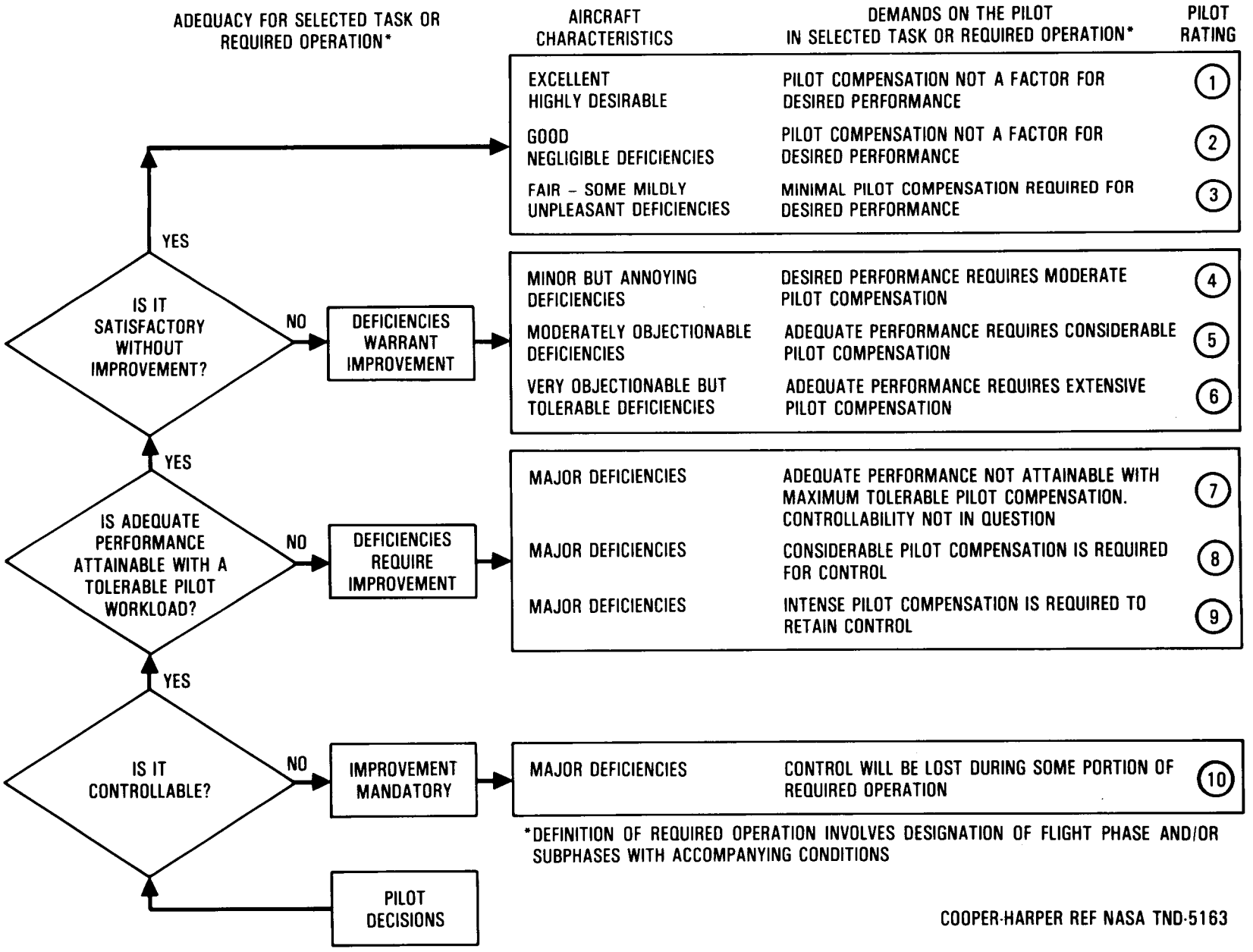

Figure 23. - Handling qualities rating scale.

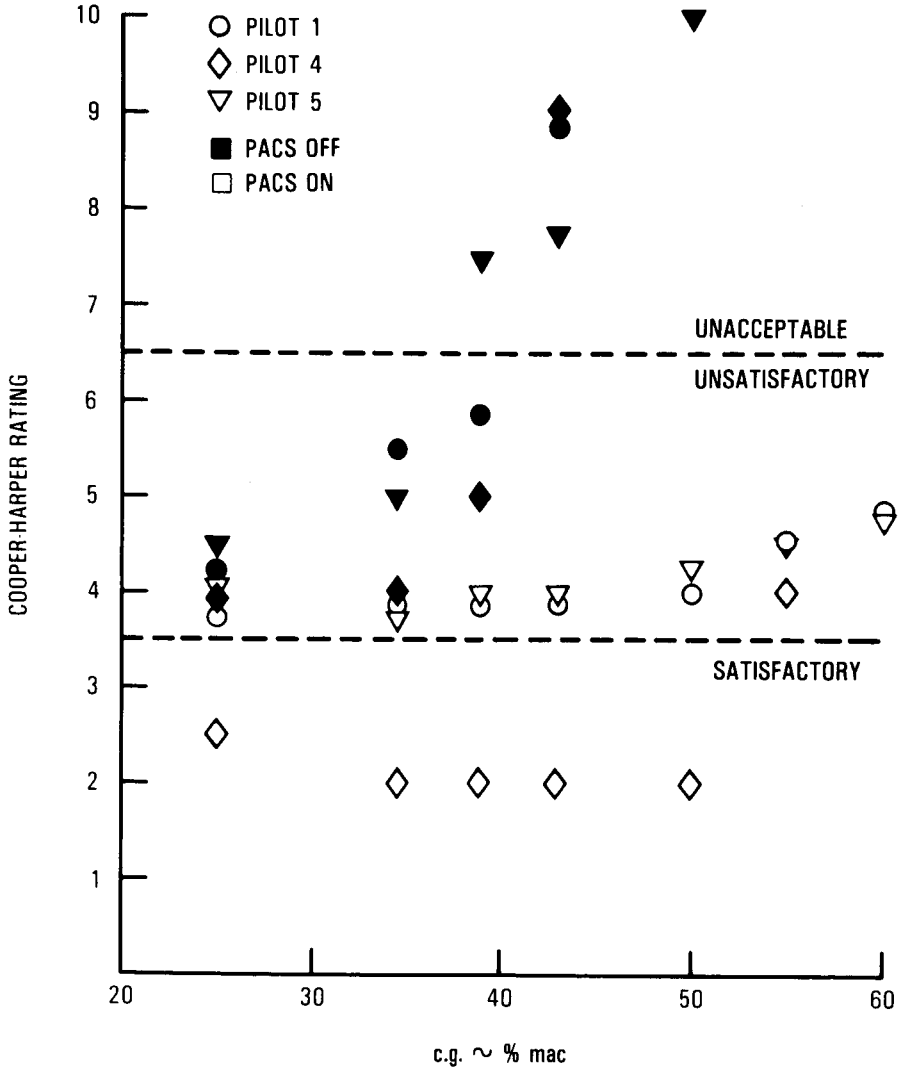

Figure 24. - Cooper-Harper ratings for flight condition 7, moderate turbulence.

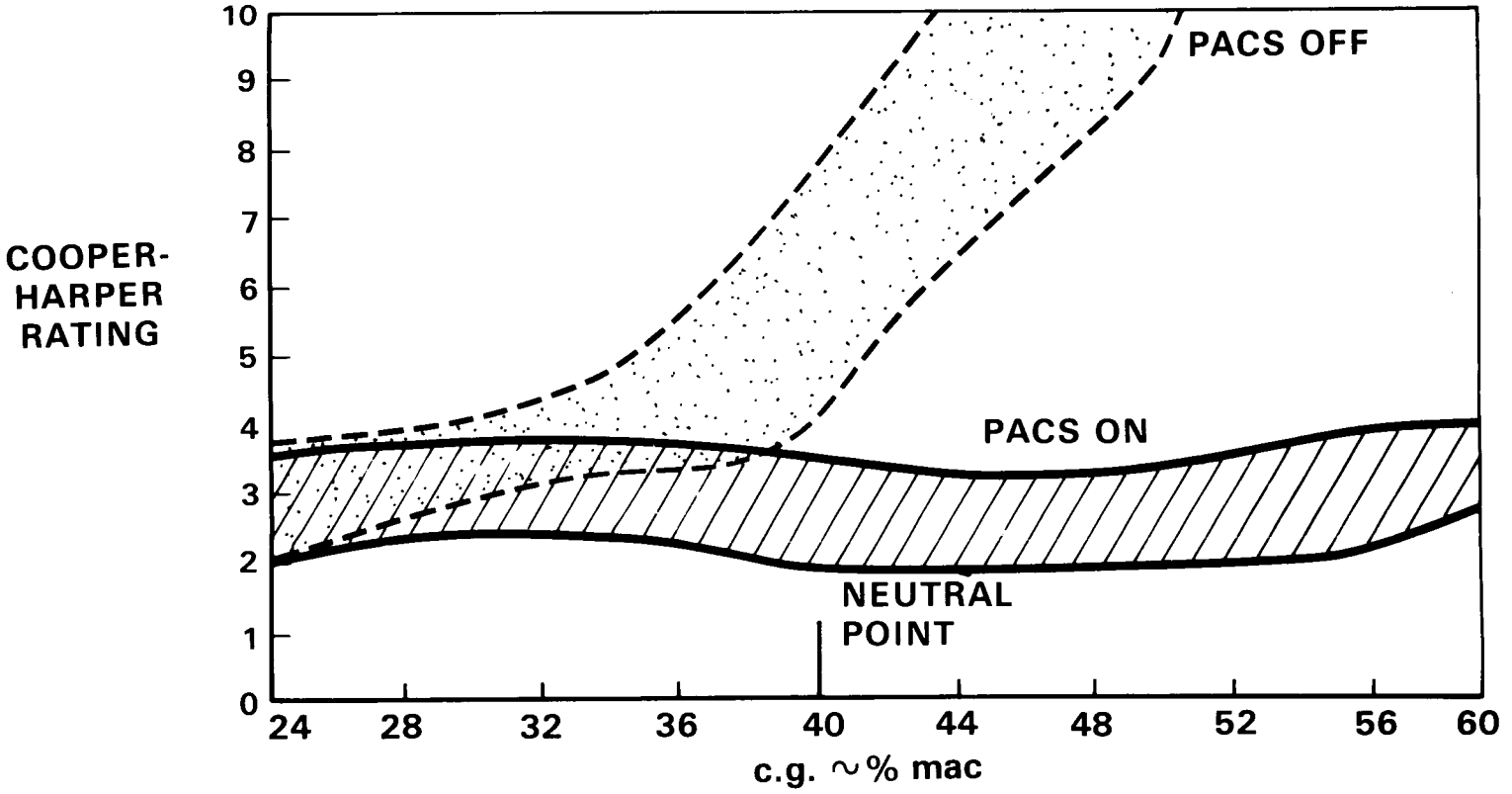

Figure 25. - Summary of advanced PACS piloted flight simulation test results

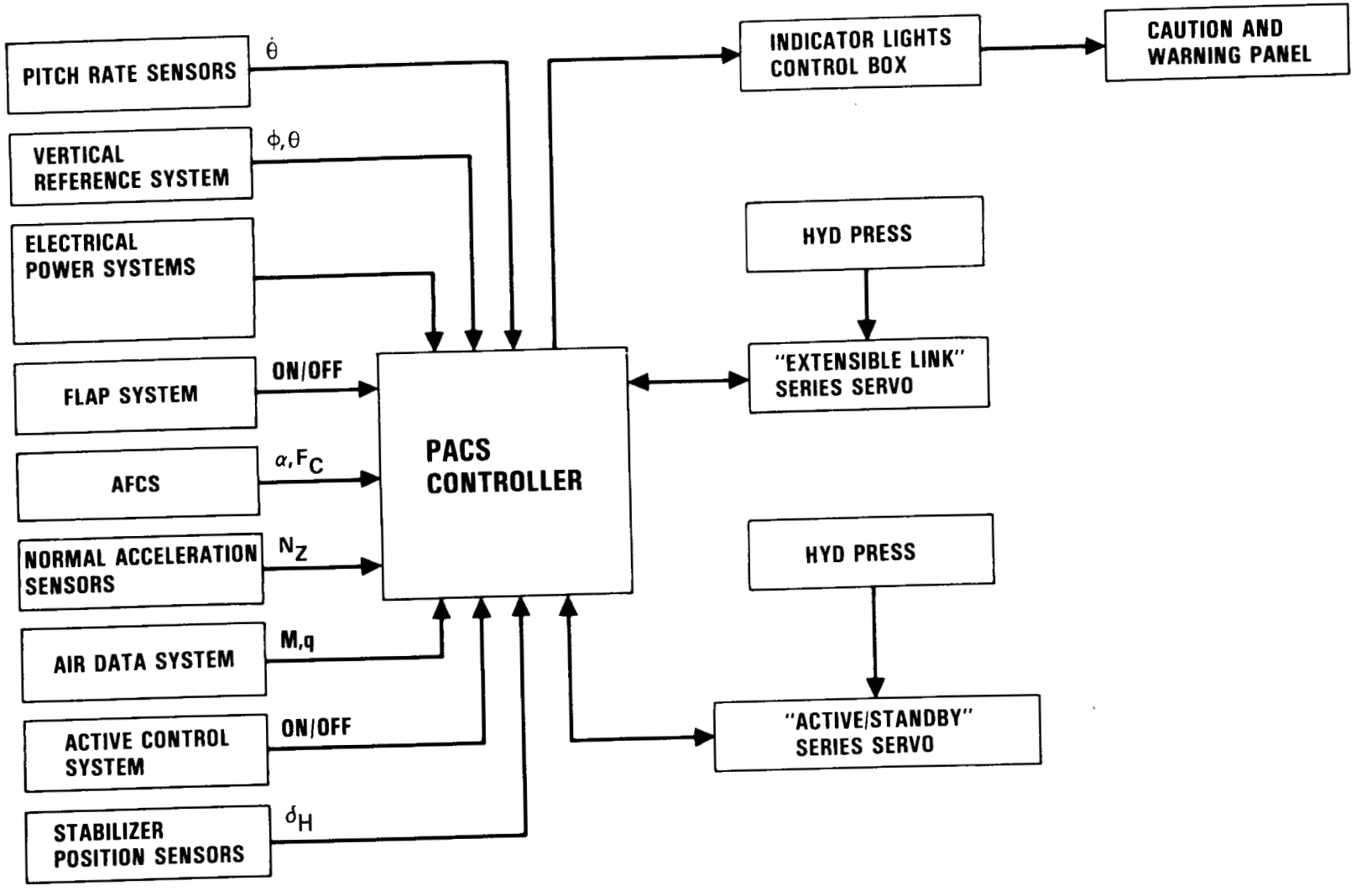

Figure 26. - Advanced PACS interface block diagram.

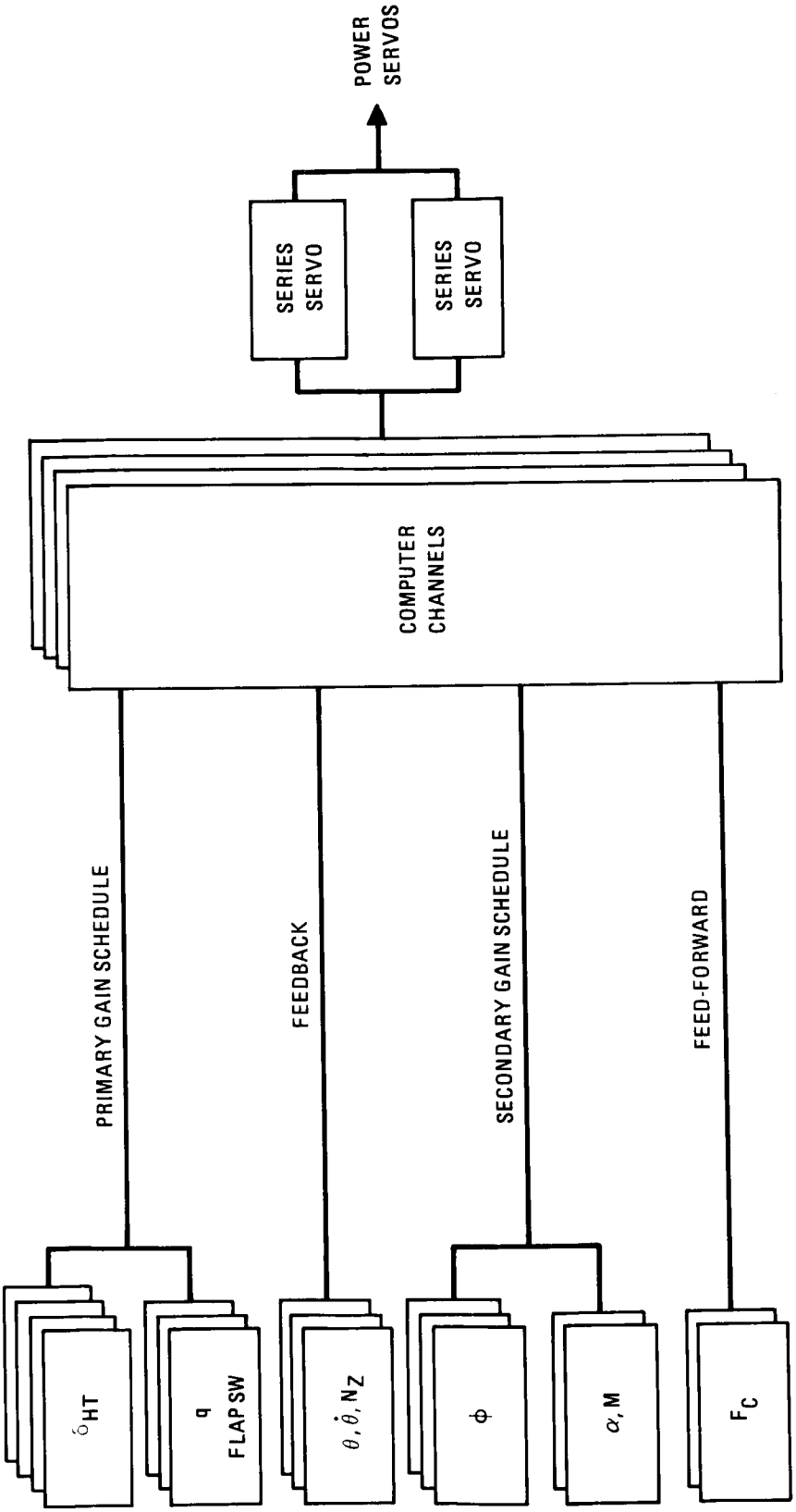

Figure 27. - Advanced PACS architecture.

3. REDUCED AREA HORIZONTAL TAIL

The small tail program objective was to determine the maximum drag benefit that can be achieved by reducing the horizontal tail area which is consistent with moving the c.g. range aft and the controllability requirements. The reduced area horizontal tail development tasks were: design criteria definition, refinement of analysis methods, and wind tunnel tests.

3.1 Design Criteria

Design criteria for a reduced area horizontal tail include high-speed and low-speed characteristics. The objective of the tail design definition was to select an airfoil which is a satisfactory compromise between the high-speed and low-speed objectives.

3.1.1 High-Speed design criteria.- The high speed design requirements were:

- Section drag characteristics shall be similar to the standard L-1011 Tail drag
- No tail drag rise shall occur within the cruise Mach number range
- Maximum lift-to-drag ratio of the tail shall occur a nominal cruise trim load.

3.1.2 Low-Speed design criteria.- The low speed design requirements were:

- Achieve nose wheel liftoff at forward c.g. for prescribed nose wheel liftoff speeds.
- Have sufficient control power to stall at forward c.g.
- Have sufficient control power for stall recovery at aft c.g.

3.1.3 Specific design requirements.- Specific small horizontal tail design requirements were:

- Takeoff nose wheel liftoff at forward c.g. with maximum takeoff flaps at the lesser of 1.05 minimum control speed or the FAA stall speed
- Control-to-stall at forward c.g. with maximum landing flaps (42 deg) and idle thrust

- At least 4.58 deg/sec^2 nose-down pitch acceleration for stall recovery at aft c.g. and at the FAA stall speed for maximum landing weight
- At least neutral stability at aft c.g.
- A c.g. range equal to that of the standard L-1011 (12 to 35 percent mac) which is 67.5 inches for aircraft weights of 338,000 pounds.

3.2 Small Tail Configurations Evaluated

The small tail configurations that were evaluated are listed below.

H_{16} - Small tail, standard fuselage (L-1011-1) length, Wortmann Airfoil (MFX 69-H-098-090-1)

H_{17} - Small tail, short fuselage (L-1011-500) length, RSS2 Airfoil configuration

H_{18} - Small tail, short fuselage (L-1011-500) length, RSS2 Airfoil configuration

H_{19} - Small tail, NASA configuration

H_{8C} - Reference tail, standard L-1011

Figure 28 shows plan views of the horizontal tails and Table 8 gives comparative geometric data.

3.3 Small Tail Design Procedures

A conventional airplane horizontal tail is sized to provide a specified margin of static stability and the required longitudinal control by having an adequate $C_{L_{max}}$ in down lift. The requirement for a specific positive margin of static stability results in a large stabilizer surface and forward center-of-gravity range which penalize performance in terms of drag and weight.

If a pitch active control system is incorporated into the airplane to provide static stability artificially, then the horizontal tail can be sized to provide the required pitch control by using the tail maximum lift capability in both the up and down directions.

Analysis methods used for analyzing the different small horizontal tail configurations are discussed in the following sections.

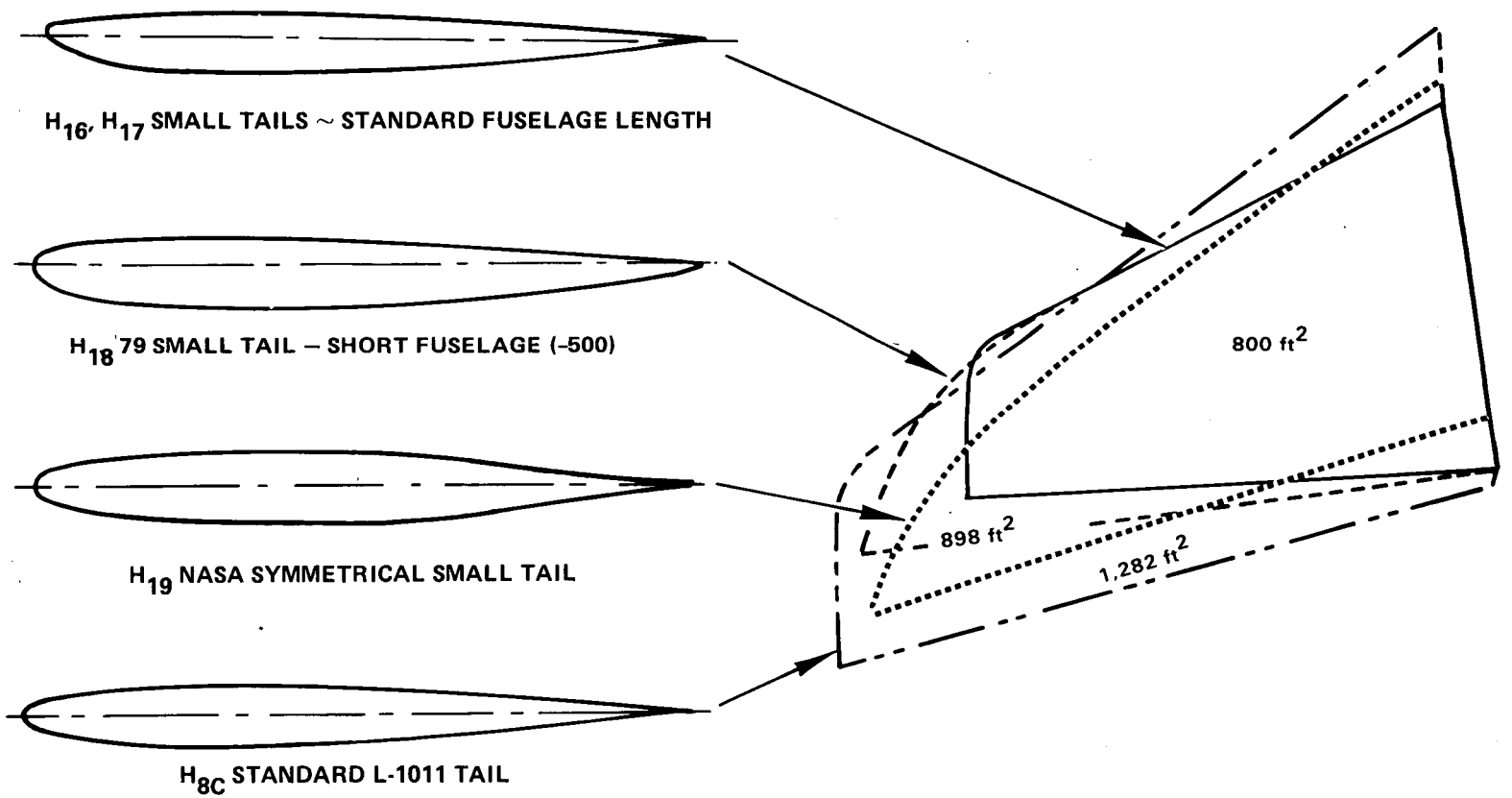

Figure 28. - Small horizontal tail configurations evaluated.

TABLE 8. - SMALL HORIZONTAL TAIL COMPARATIVE DATA

	H_{8c} Standard	H_{16} Small	H_{17} Small	H_{18} Small	H_{19} Small
Aspect ratio	4	4	4	4.5	4.5
Taper ratio	0.33	0.33	0.33	0.33	0.33
Camber	0	0.013 mac	0.016 mac	0.016 mac	0
Leading-edge radius	0.0089 mac	0.006 mac	0.036 mac	0.036 mac	0.015 mac
Thickness ratio	0.09	0.09	0.1045	0.1045	0.10
Quarter chord sweep	35 deg	28 deg	25 deg	25 deg	35 deg
Total Area ft^2	1282	800	800	898	898
Exposed Area ft^2	960	552	552	652	644
Exposed/Total	0.75	0.69	0.69	0.73	0.72
Elevator chord ratio	0.25 mac	0.3 mac	0.3 mac	0.3 mac	0.3 mac
Stabilizer throw	15 deg	20 deg	20 deg	17 deg	17 deg
Elevator throw	25 deg	40 deg	40 deg	35 deg	35 deg

3.3.1 H_{16} Horizontal tail analysis.- The H_{16} tail development was the initial effort to develop a small L-1011 horizontal tail and was accomplished with Lockheed funds (Reference 6). This work is summarized in this report to provide a foundation of the work that was accomplished under the ACEE contract.

A helicopter rotor blade airfoil (Wortmann MFX 69-H-098-090-1, Reference 7) was selected and slightly modified for the small tail airfoil because of its good high-speed and high-lift characteristics. The reduction in aerodynamic drag was estimated by using standard handbook methods for lifting surfaces. A form factor for the airfoil thickness was applied to the planar surface compressible skin friction drag which was computed by the Sommer and Short T' method. The form factor was determined by a special Lockheed correlation of airfoil drag with thickness ratio.

The analysis showed that the small horizontal tail (800 ft^2 area) drag reduction was 11 drag counts at wind tunnel test conditions and 7 counts at full-scale cruise conditions. This represented a potential drag savings of 2.7 percent at nominal cruise conditions. The net improvement in cruise efficiency would be approximately three percent due to the weight reduction of the smaller horizontal tail.

3.3.2 H_{17} Horizontal tail analysis.- Advanced airfoil technology was used to design a relative thick airfoil with large leading-edge radius to provide lift at low speed for controllability without degrading high speed drag characteristics. Pressure distribution of the H_{17} airfoil (designated RSS2 Airfoil) was determined by using the Jameson-Caughey exact potential inviscid flow analysis code, Flow 22 (References 6 and 7). A fully automated curvature airfoil shaping design system (Figure 29) was used to optimize the small tail airfoil.

3.3.3 H_{18} Horizontal tail analysis.- This small horizontal tail (898 ft^2 area) is a common size tail for both short-body and long-body L-1011 derivatives. The design goal was to provide a $C_{L_{max}} = -1.4$ for full scale flight conditions. The handbook methods used for predicting drag of the H_{16} tail were 27 percent lower than measured in the wind tunnel even though the same method had predicted drag of the standard L-1011 tail (H_{8C}) correctly. Therefore, drag of the H_{18} tail was estimated by applying an exposed area correction to previous wind-tunnel test results of the H_{16} tail.

The estimation showed that the L-1011 drag would be reduced by about 6 counts at wind tunnel test conditions. Thus, a two percent L/D benefit was predicted based on reduced area and lower weight of the tail.

3.3.4 H_{19} Horizontal tail analysis.- A review of independent development of small horizontal tail designs by NASA and Lockheed revealed significant differences. The following differences were identified:

	NASA	Lockheed
Sweep Angle (mac/4)	32.5 deg	25 deg
Aspect Ratio	3.0	4.5
Airfoil Sections	NASA developed inverse camber & symmetrical	Lockheed Developed inverse camber
Airfoil Thickness	10%	10.5%

After reviewing the data it was concluded that drag creep problem encountered with the Lockheed configuration could be eliminated by: 1) increasing the sweep angle of the tail, 2) using one of the NASA airfoil sections which is one-half percent thinner, and 3) retaining the 4.5 aspect ratio planform. Of the two NASA airfoils, the symmetrical section was selected because of its good low-speed properties.

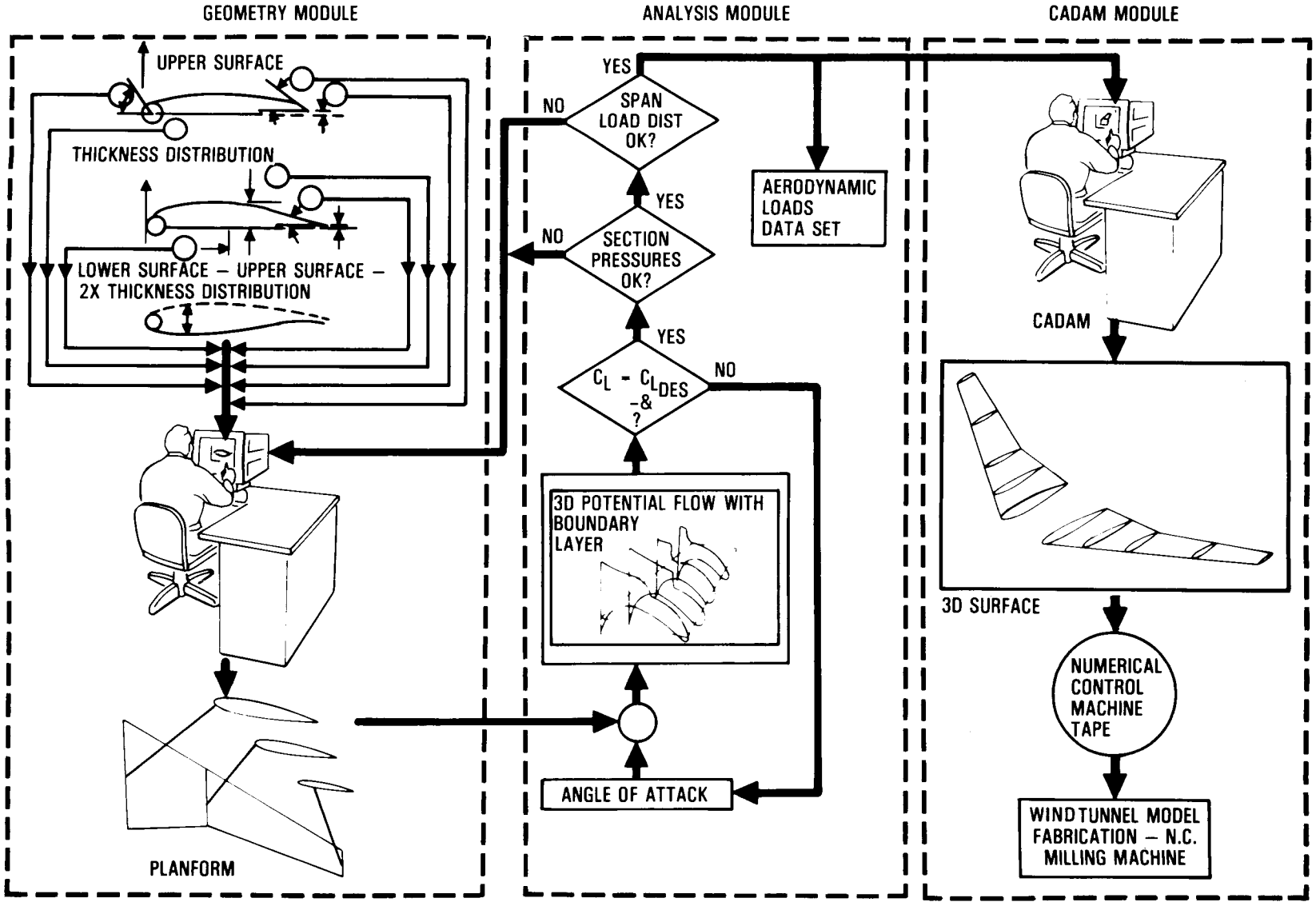

Figure 29. - Curvature airfoil shaping design system.

It was further decided to determine an appropriate sweep angle for the horizontal tail by means of viscous Jameson-Caughey analysis, and based on the results of that analysis to proceed with high-speed model construction and testing.

3.4 Wind Tunnel Tests

Small tail wind tunnel tests which were performed are listed in Table 9. The H_{16} tests were Lockheed funded, the H_{17} tests were funded by the first ACEE active control technology contract awarded to Lockheed (NAS1-14690). The remainder of tests were funded under the current contract (NAS1-15326). The wind tunnel test results is discussed in the next section.

3.5 Wind Tunnel Test Results

The small horizontal drag benefits and high lift characteristics are presented in Figures 30 and 31 respectively.

The H_{16} tail shows a drag count reduction of 7 (Figure 30) over the cruise range of Mach .8 to .83. However, the low-speed high-lift characteristics did not meet the $C_{L_{max}} = -1.4$ target (Figure 31).

The H_{17} tail low-speed high-lift characteristics did not meet the $C_{L_{max}}$ target. Consequently, high speed tests were not performed.

The H_{18} tail drag count reduction at Mach .8 was about 5 drag counts, but a drag creep occured throughout the Mach range. The $C_{L_{max}}$ target was achieved.

The H_{19} tail shows a drag count reduction of 7 and a $C_{L_{max}} = -1.2$. The drag reduction and corresponding weight of the H_{19} tail provides an estimated L/D benefit of two percent. Use of the H_{19} tail on an L-1011 requires the forward c.g. limit be restricted. Use of this tail on a next generation transport may be feasible if the aircraft is equipped with a PACS and has a properly designed c.g. range.

TABLE 9. - SMALL HORIZONTAL TAIL WIND TUNNEL TESTS

Date	Test No.	Wind Tunnel	Type of Test	H_{8C}	H_{16}	H_{17}	H_{18}	H_{19}
Apr 76*	N-307	Calspan 8 ft TPT	Limited High-Speed Force Data in Cruise-No Elevator		X			
Nov 76*	L-404	Calac LSWT	Low-Speed Force Data at Low Reynolds Number	X	X			
Nov 78**	L-429	Calac LSWT	Low-Speed Force & Pressure Data at Low Reynolds Number			X		
Mar 79**	L-442	Calac LSWT	Complete Low-Speed Force Data at Low Reynolds Number			X		
July 79	N-336	Langley 8 ft TPT	Complete High-Speed Force & H.T. Pressure Data	X			X	
Sept 79	N-340	Calspan 8 ft TPT Data	Complete High-Speed Force & H.T. Pressure	X			X	
Jan 80	N-337	Ames 12 ft PT	Complete Low-Speed Force Data at High Reynolds Number	X			X	
Feb 80	S-387	Calac 4 ft T/ST	Horizontal Tail Drag at Cruise Mach Number	X	X	X	X	
Aug 81	N-369	Calspan 8 ft TPT	Complete High-Speed Force Data at Cruise Mach Number					X
Jan 82	N-337	Ames 12 ft PT	Low-Speed Force Data at High Reynolds Number					X

*Lockheed Funded

**NASA Contract NAS1-14690

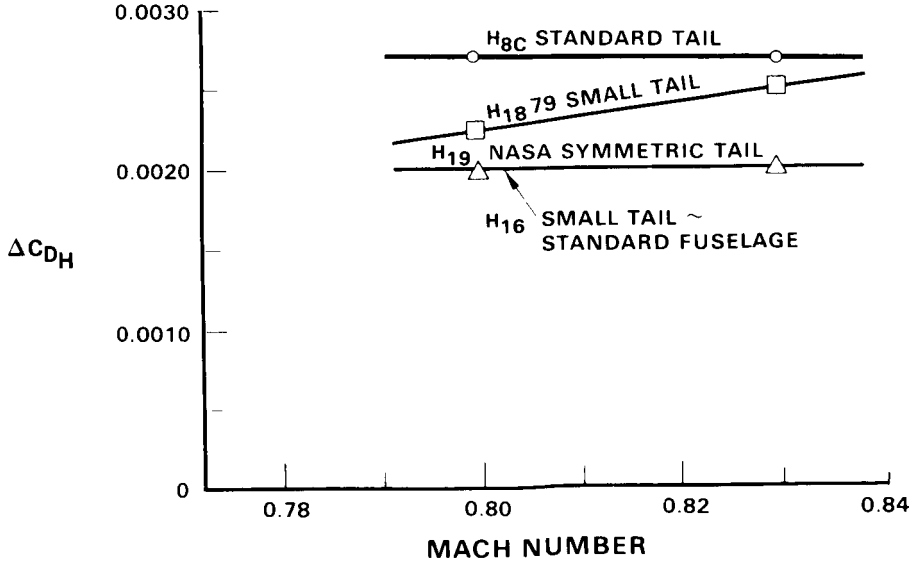

Figure 30. - Horizontal tail drag characteristics.

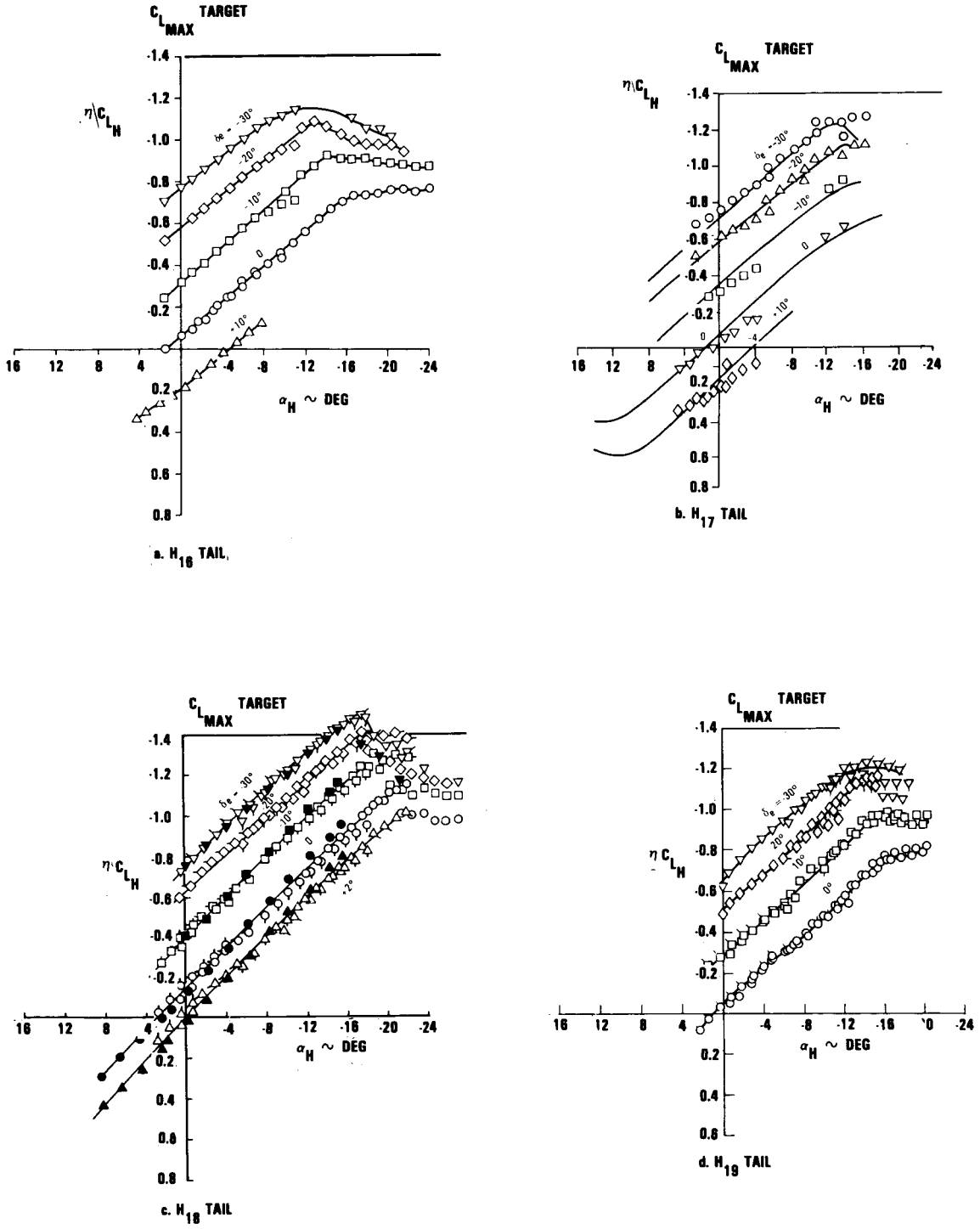

Figure 31. - Comparison of small horizontal tail high-lift characteristics.

CONCLUSIONS

This program has demonstrated by piloted flight simulation tests (based on L-1011 aerodynamic data) that an advanced PACS will provide handling qualities at negative stability margins up to 20 percent which are equivalent to the handling qualities of the baseline airplane at a positive 15 percent stability margin. Also, it has shown that the modal control method of modern control theory can be used for control law synthesis of a multiple feedback loop PACS and provides a valid control law to control the dynamic stability. The piloted flight simulation tests demonstrated that the PACS requires a feed-forward loop to provide the desired control column gradients for maneuver stability and a Mach compensation loop to provide the desired column forces for speed stability.

The small horizontal tail program has demonstrated by wind tunnel tests that a 30 percent tail area reduction (relative to standard L-1011 tail) provides an increase in cruise efficiency of about two percent and that a 38 percent tail area reduction provides an increase in cruise efficiency of about three percent. However, forward c.g. limitations would have to be imposed on the aircraft because the maximum horizontal tail lift goal was not achieved and sufficient aircraft nose-up control authority was not available. This limitation would not be required for a properly designed new aircraft.

Potential fuel savings for a future transport aircraft that has a small horizontal tail and flies at negative static stability margins would be about six percent. This ariplane would have to be equipped with a high-reliability PACS to provide satisfactory handling qualities.

REFERENCES

1. Urie, D.M., "Acceleration Development and Flight Evaluation of Active Controls Concepts for Subsonic Transport Aircraft - Volume II: Aft CG Simulation and Analysis," NASA CR 159098, September 1979.

2. Guinn, W.A., "Development and Flight Evaluation of an Augmented Stability Active Controls Concept," NASA CR 165951, September 1, 1982.

3. Guinn, W.A., Willey, C.S., and Chong, M.G., "Extended Flight Evaluation of a Near-Term Pitch Active Controls System," NASA CR 17226, December 21, 1983.

4. Rising, Jerry J., "Development of a Reduced Area Horizontal Tail for a Wide Body Jet Aircraft," NASA CR-172278, February 1, 1984.

5. Urie, D.M., and Passer, J.S., "Aerodynamic Development of a Small Horizontal Tail for an Active Control Released Stability Transport Application," AIAA Paper 79-1653, August 6, 1979.

6. Bingham, Gene J., and Noonan, Kevin W., "Low Speed Aerodynamic Characteristics of Five Helicopter Blade Sections at Reynolds Numbers from 2.4×10^6 to 8.4×10^6, " NASA TMX-2467, 1972.

[redacted]

1. Report No.	2. Government Accession No.	3. Recipient's Catalog No.
NASA CR - 172283		

4. Title and Subtitle	5. Report Date
Development of a Advanced Pitch Active Control System and a Reduced Area Horizontal Tail for a Wide-Body Jet Aircraft Executive Summary	February 1, 1984
	6. Performing Organization Code

7. Author(s)	8. Performing Organization Report No.
Wiley A. Guinn	LR 30463
	10. Work Unit No.
9. Performing Organization Name and Address	
Lockheed California Company Burbank, CA	11. Contract or Grant No. NAS1-15326
	13. Type of Report and Period Covered Contractor Report Dec 1978-April 1983
12. Sponsoring Agency Name and Address	
National Aeronautics and Space Administration Washington, D.C. 20546	14. Sponsoring Agency Code

15. Supplementary Notes

Langley Technical Monitor: Dennis W. Bartlett

16. Abstract

This report documents work that was accomplished toward development of a advanced pitch active control system (PACS) and a reduced area horizontal tail for a wide-body jet transport (L-1011) with a flying horizontal stabilizer. The advanced PACS control law design objectives were to provide satisfactory handling qualities for aft c.g. flight conditions to negative static stability margins of 10 percent and to provide good maneuver control column force gradients for nonlinear stability flight conditions. Validity of the control laws were demonstrated by piloted flight simulation tests on the NASA Langley Visual Motion Simulator. Satisfactory handling qualities were actually demonstrated to a negative 20 percent static stability margin. The PACS control laws were mechanized to provide the system architecture that would be suitable for an L-1011 flight test program to a negative stability margin of 3 percent which represents the aft c.g. limits of the aircraft. Reduced area horizontal tail designs of 30 and 38 percent with respect to the L-1011 standard tail were designed fabricated and wind tunnel tested. Drag reductions and weight savings of the 30 percent smaller tail would provide an L/D benefit of about 2 percent and the 38 percent small tail L/D benefit would be about 3 percent. However, forward c.g. limitations would have to be imposed on the aircraft because the maximum horizontal tail lift goal was not achieved and sufficient aircraft nose-up control authority was not available. This limitation would not be required for a properly designed new aircraft.

17. Key Words (Suggested by Author(s))	18. Distribution Statement
Active Control System, Control System, Pitch Control, Longitudinal Control, Aircraft Fuel Savings	[redacted]

19. Security Classif. (of this report)	20. Security Classif. (of this page)	21. No. of Pages	22. Price*
Unclassified	Unclassified	62	